AC corrosion on cathodically protected steel

Andreas Torstensen

I hereby declare that this work has been carried out independently and in compliance with the examination regulations of the Norwegian University of Science and Technology, NTNU.

_____

Andreas Torstensen

Trondheim, June 2012

Preface

This work is the master thesis of the author and a basis for the evaluation of the course TMT 4905 at the Norwegian University of Science and Technology, NTNU. The work has been based on a collaboration between NTNU and Statoil and the background of the work is the introduction of the Direct Electric Heating system (DEH).

First of all, I would like to thank my supervisor, Professor Kemal Nisancioglu. He has guided me through the material of AC corrosion and has been very helpful and a great inspiration. Nisancioglu has always been available when I have asked about meetings and discussions.

I would also give large thanks to my co-supervisor, Sven Morten Hesjevik at Statoil for his useful comment and ideas. Hesjevik has supported me with materials and equipment to do this work.

At last I would like to thank my fellow graduate students at material science, NTNU. I have had an amazing time here in Trondheim and both the studies and the time here in Trondheim in general have been much easier with such fantastic people around.

Andreas Torstensen

Trondheim, June 2012

Abstract

This report deals with the effect of alternating current on cathodically protected steel. AC corrosion has become relevant in the offshore industry due to the introduction of the direct electric heating system (DEH). The principle with DEH is to prevent wax solidification inside pipelines by heating them up with alternating current. This can give rise to AC corrosion.

DC current densities, AC current densities and DC potential have been measured for steel samples under cathodic protection with applied AC voltage. Weight loss measurements were done of both steel and sacrificial anode samples after the experiments. There have also been focused on the corrosion kinetics of AlZnIn by plotting polarization curves and potential measurements over time with applied AC current.

The weight loss measurements have shown that carbon steel is protected against AC corrosion for AC current densities lower than 1300 A/m^2. All steel samples had corrosion rate lower than 0,1 mm/year up to this value. SEM investigation showed that no pitting corrosion occurred at any of the steel surfaces. The corrosion rate of AlZnIn increased with increasing AC current density up to 300 - 500 A/m^2. At higher AC current density, the sacrificial anodes became passive which resulted in decreased protection current and corrosion rate. Polarization curves of AlZnIn have also shown large resistance when AC is introduced which is probably due to surface coverings.

Study of the surface morphology of AlZnIn have shown that more localized corrosion occurs with increasing AC current. At 500 A/m^2 pitting corrosion occurred at the whole surface and the pits became deeper with increasing AC. This resulted in decreased efficiency of the sacrificial anode and consequently reduced DC current density and corrosion rate of the sacrificial anode.

Potential and current measurements have shown that the galvanic potential of steel and AlZnIn became more electropositive with increasing AC current density. It is believed that this is due to more localized corrosion with increasing AC voltage and consequently lowering of the anode/cathode ratio. This will force the potential to more anodic values. The initial DC current density increased with increasing AC voltage for all samples but the passivation of sacrificial anode resulted in high reduction rate with time. Polarization curves of AlZnIn showed that the corrosion potential decreased and the corrosion current increased when AC was introduced. Within the samples exposed to AC there were no significant difference in corrosion potential and corrosion current.

Sammendrag

Denne rapporten tar for seg effekten av vekselstrøm på katodisk beskyttet stål. AC korrosjon har blitt relevant i offshoreindustrien på grunn av innføringen av Direct electric heating system (DEH). Prinsippet med DEH er å forhindre at voks og hydrater størkner i rørledninger ved å varme dem opp med vekselstrøm. Dette kan forårsake AC korrosjon.

DC strømtetther, AC strømtetther og DC potensial har blitt målt for stålprøver som har vært under katodisk beskyttelse med påtrykt AC spenning. Det har blitt gjort vekttapsmålinger på både offeranodene og stålprøvene etter forsøkene. Det har også vært fokus på korrosjonskinetikken ved AlZnIn ved å plotte polarisasjonskurver og målinger av korrosjonspotensialet over tid med påtrykt AC spenning.

Vekttapsforsøkene viste at stål er beskyttet mot AC korrosjon for AC strømtettheter under 1300 A/m^2. Alle stålprøvene hadde lavere korrosjonshastigheter enn 0,1 mm/år under denne verdien. Undersøkelser i SEM viste at det heller ikke var noe gropkorrosjon på noen av stålprøvene. Korrosjonshastigheten på AlZnIn økte med økende AC strømtetthet helt opp til 300 - 500 A/m^2. Ved høyere verdier av AC strømtetthet ble offeranoden passiv, noe som resulterte i minkende beskyttelsestrøm og korrosjonshastighet. Polarisasjonskurvene for AlZnIn viste at det er stor motstand i kretsen når AC er involvert, noe som trolig skyldes belegg på overflaten.

Undersøkelser av overflatemorfologien på AlZnIn viste at det blir mer lokalisert korrosjon med økende AC strøm. Ved 500 A/m^2 forekom det gropkorrosjon på hele overflaten og disse gropene ble dypere med økende AC. Dette resulterte i mindre effektive offeranoder og dermed redusert DC strømtetthet og korrosjonshastighet på offeranoden.

Målinger av potensial og strøm har vist at det galvaniske koblingspotensialet mellom stål og AlZnIn blir mer elektropositivt med økende AC strømtetthet. Dette skyldes trolig at det blir mer lokalisert korrosjon med økende AC spenning og dermed lavere anode/katode forhold. Dette fører til at potensialet går mot mer anodiske verdier. DC strømtettheten ved forsøkenes start økte med økende AC spenning for alle prøvene, men passiveringen av offeranodene førte til at strømtettheten ble redusert med tiden. Polarisasjonskurvene for AlZnIn viste at korrosjonspotensialet sank og korrosjonstrømtettheten økte når AC ble involvert. For de prøvene som ble eksponert mot AC var det ingen tydelig forskjell i korrosjonspotensial og korrosjonstrømtetthet.

Contents

Chapter 1

Introduction

Cathodic protection is the most usual way to protect offshore installations against corrosion. Polarization of the steel due to cathodic protection will result in an increase of pH at the metal surface. This will lead to formation of calcareous deposits which plays a significant role in the corrosion protection. The current demand from the sacrificial anode will decrease which gives the anodes an increased lifetime.

When a hydrocarbon production pipeline is shut down, it cools to a temperature where the hydrates solidify and this may block the pipe flow. To prevent this problem, the direct electric heating system (DEH) has been installed on pipelines in the North Sea since 2000. DEH is a system where alternating current (AC) is applied to increase the temperature due to resistance in the pipelines. This will result in current transfer from the pipelines to the sea which can lead to AC corrosion.

After the first case of AC corrosion of a cathodically protected pipeline in the field was identified in Germany in 1986, the subject has reached increased attention the last couple of years. However, the results in the studies are often contradictory and there is not a satisfied explanation of AC corrosion on cathodically protected steel available. A master thesis from Line Sunde Lilleby written at NTNU in autumn 2009 [1] was the only written work on the effect of AC current on calcareous deposits found. No written work on the effect of AC current on AlZnIn alloys has been found. This project is a continuation of the experiment performed in Lilleby's studies.

The purpose of this project is to investigate the protection properties of calcareous deposits and also the effect of applied AC current on cathodically protected carbon steel. The focus will be on the corrosion mechanisms on both carbon steel and AlZnIn sacrificial anodes and the protection potential and current variation. Carbon steel samples will be pre exposed to cathodic protection to form calcareous deposits. Each of the samples will then be exposed to cathodic protection with different values of applied AC voltages. Protection potential, protection current, AC current and corrosion rates of both carbon steel and AlZnIn will be measured during the test period. There will also be made polarization curves of AlZnIn and the potential variation with time will be measured for this alloy. The surface of the steel and AlZnIn samples will also be investigated in SEM.

Chapter 2

Theory

This chapter describes the already existing theory of AC corrosion on cathodically protected steel and calcareous deposits. There are not much existing theory of the effect of AC current on AlZnIn. Theory of AlZnIn alloy itself and the effect of AC on pure Aluminum is therefore included in this chapter.

2.1 Cathodic protection

Cathodic protection (CP), often combined with a coating system, is the most usual way to protect carbon steel from corrosion in offshore environment. The principle of CP is that an external current is supplied to the steel which polarizes the steel to a potential more negative than its protection potential as can be seen from Figure 2.1. This is done either by sacrificial anodes or an impressed current system. CP from sacrificial anodes is based on the principle of galvanic corrosion where a less noble metal is connected to the structure to be protected. To achieve protection, a potential E_p -850 mV_{SCE} is needed for carbon steel in seawater [1].
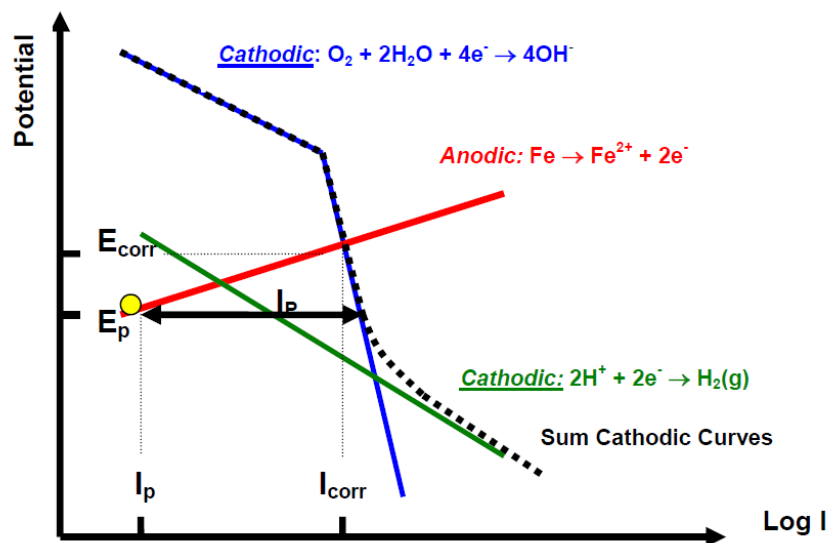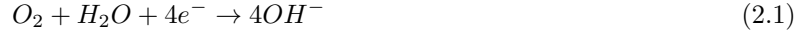

Figure 2.1: Sketch of a potential-current diagram showing how the steel is polarized by the protection current [1].
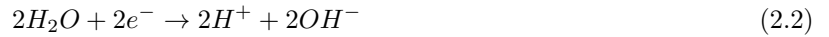
2.2 Calcareous deposits

2.2.1 Precipitation and formation of calcareous deposits

For most cathodic protection systems in seawater, the principal cathode reaction is:

$$O_2 + H_2O + 4e^- \rightarrow 4OH^- \tag{2.1}$$

In cases where the potential is more negative than the reversible hydrogen potential, production of hydrogen becomes possible:

$$2H_2O + 2e^- \rightarrow 2H^+ + 2OH^- \tag{2.2}$$

It has been reported that below -1000 mV_{SCE}, hydrogen evolution will be the dominant reduction reaction [2]. Reaction (2.1) and (2.2) will produce hydroxyl ions and the pH will increase in the diffuse layer where the equilibrium reactions can be quite different from the reactions in the bulk seawater conditions. In seawater, pH is controlled by the following reactions:

$$CO_2 + H_2O \rightarrow H_2CO_3 \tag{2.3}$$

$$H_2CO_3 \rightarrow H^+ + HCO_3^- \tag{2.4}$$

$$HCO_3^- \rightarrow H^+ + CO_3^{2-} \tag{2.5}$$

If pH increases due to cathodic protection, the following reactions are possible:

$$CO_2 + OH^- \rightarrow HCO_3^- \tag{2.6}$$

$$OH^- + HCO_3^- \rightarrow H_2O + CO_3^{2-} \tag{2.7}$$
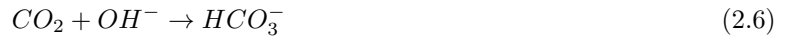
This may result in precipitation of calcareous deposits:

$$CO_3^{2-} + Ca^{2+} \rightarrow CaCO_3 \tag{2.8}$$

When OH^- is introduced due to cathodic protection, equations (2.4) - (2.5) are displaced to the right. This opposes any rise in the pH and accounts for the buffering capacity of seawater. However, equation (2.3) - (2.8) indicates that this buffering action is accompanied by the formation of calcareous deposits on cathodic surfaces exposed to seawater [3].

Magnesium compounds may also precipitate at the surface [4]:

$$Mg^{2+} + 2OH^- \rightarrow Mg(OH)_2 \tag{2.9}$$

However, magnesium hydroxide is unsaturated in seawater and less stable than calcium carbonate which will precipitate at a pH of 7,5 [5]. For magnesium hydroxide to precipitate, pH needs to exceed approximately 9,5 [3]. Barchiche et al. suggested that the potential is the parameter that governs the nature of the phases formed in calcareous deposit, by controlling the pH. A deposit on carbon steel containing both $CaCO_3$ and $Mg(OH)_2$, could only be obtained at E = -1,2 V_{SCE} [4]. It is generally agreed that a thin magnesium rich inner layer will form beneath an outer layer of aragonite [5].

2.2.2 Microstructure of calcareous deposits

Calcium carbonate occurs in the ocean in two crystalline forms; calcite and aragonite. Calcite and magnesium carbonate have quite similar structure and these compounds will therefor form solid solutions. However, precipitation of calcite is strongly inhibited by dissolution of magnesium. Consequently, aragonite is the phase that actually forms when pH is increased by cathodic protection [3]. Mantel et al. [6] described the morphologies of the substrate according to the duration of applied CP. The initially deposited structures (15 h – 30 h) were comprised primarily of individual, isolated particles, whereas at greater times (60 h and above), these particles had grown together and covered almost the entire surface.

Due to an inhibiting influence of Mg^{2+} on aragonite, $Mg(OH)_2$ precipitates faster than $CaCO_3$ on electrode surfaces, which means that $Mg(OH)_2$ will form a thin inner layer on the surface [6]. This layer is difficult to observe, but can be detected in EXD analysis. Aragonite crystals will form a thicker layer on top of the $Mg(OH)_2$ layer [7]. Mg^{2+} will inhibit formation of aragonite, but will not prevent it as for calcite. Aragonite particles will nucleate on the Mg rich phase. Once the particles have achieved a critical size, they will grow rapidly due to the relatively high supersaturation that exists at pH = 9,5 [6]. While $Mg(OH)_2$ forms with no well defined crystals, aragonite is recognized by its flower shaped crystals [7].

2.2.3 Influence of calcareous deposits on protection current

Calcareous deposits are beneficial because it will act as a coating by reducing the oxygen access to the surface and consequently reduce the protection current required. Previous studies have shown that the current requirement decreases when the Ca/Mg ratio increases [8]. This indicates that calcium carbonate scales are more protective than magnesium hydroxide.

The amount of calcareous deposits will increase with increasing current density, reaching a maximum current density depending on the material and electrolyte. At higher current densities, the amount of calcareous deposit seems to decrease. It is suggested that this is due to increased hydrogen evolution [9].

It is generally agreed that calcareous deposits act as an effectively diffusion barrier for oxygen and will prevent oxygen reduction on the steel surface. However, calcareous deposits seem not to have a significant effect on the water reduction reaction. It is not clear how calcareous deposits block oxygen reduction and not water reduction, since both reactions are dependent on diffusion of the reactants to the reaction site [8].

Previous studies shows that current demand plotted versus time for cathodic protection in seawater is characterized by a sigmoidal curve involving an upper plateau of approximately constant current density to about 50 hours. A transition regime of current density drop is then observed at 50 to 100 hours, followed by a lower plateau of constant current density [6]. Figure 2.2 shows how current density decreases with time for carbon steel.

It has been found that deposits which formed on carbon steel in the potential range from - 0,9 V_{SCE} to -1,05 V_{SCE} was the most protective. Those that formed at more positive potentials where thinner and less dense and those that formed at more negative potentials became dislodged by hydrogen evolution [10].
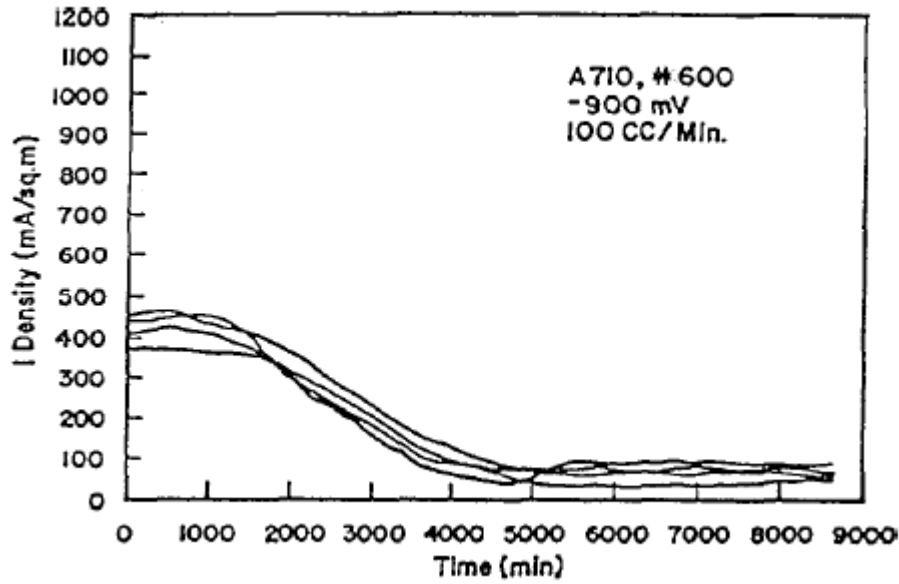
Figure 2.2: Current density vs time curve for a A710 steel polarized to -900 mV_{SCE}. The different curves represent different surface treatment [6]

2.2.4 Effect of temperature on calcareous deposits formation

The composition, thermodynamics and kinetics of seawater are dependent of temperature. The surface coverage of calcareous deposits at low temperature is much smaller than that in room temperature, which means that deposits formed at low temperatures have a less protective effect. This can be explained by the smaller reaction rate constant (K_{CaCO_3}) and reaction order (m_{CaCO_3}) at lower temperatures compared to room temperature, as shown in Table 2.1. The high solubility constant ($K_{sp,CaCO_3}$) will also reduce the formation rate of calcareous deposits at low temperature [11].

Table 2.1: Parameters of precipitation reaction and homogenous reaction at different temperatures at 35 ppt salinity [11].

Parameter	25ºC	15ºC	5ºC
$K_{sp,CaCO_3} \times 10^{13}(mol^2/cm^6)$	9,14	9,78	10,4
$K_{sp,Mg(OH)_2} \times 10^{19}(mol^3/cm^9)$	4,50	3,65	2,80
$K_{CaCO_3} \times 10^{13}(mol/cm^2 \cdot s)$	11,3	9,77	4,0
$K_{Mg(OH)_2} \times 10^7(cm^7/mol^2 \cdot s)$	3,7	2.85	2,0
m_{CaCO_3}	1,7	1,0	0,4
$K_{eq} \times 10^{-8}(cm^3/mol)$	0,84	1,36	2,36

While the solubility constant for $CaCO_3$ increases with decreasing temperature, the solubility constant for $Mg(OH)_2$ will act in the opposite way. This indicates that the Ca/Mg ratio will decrease with decreasing

6

temperature and this will result in Mg^{2+}rich calcareous deposits. The protectiveness of this layer is poor, due to high porosity [11].

2.2.5   Effect of flow rate on formation of calcareous deposits

The thickness off the diffusion layer is the main parameter that is affected by flow velocity. For increasing flow velocity, the diffusion layer becomes thinner and the cathodic current density will increase. Although the current density increases, thinner diffusion layer also promotes the diffusion of OH^- ions back to the bulk solution. Also the mass flux of HCO_3^- increases due to convection and consumes more OH^- in reaction (2.8). Consequently, the pH on the electrode surface does not increase much with increasing flow rate. As a result, higher flow velocity makes little contribution to the formation of calcareous deposits, even though the cathodic current density increases. Previous work has shown that high flow velocity will not remove the calcareous deposit. However, higher velocity may be harmful to the nucleation of $CaCO_3$ and $Mg(OH)^-$. Therefore, high velocity flow has no advantages on the formation of calcareous deposits [11].

2.3   Effect of AC signal on DC signal

When an electrical circuit is driven by more than one independent source of energy, the total response is the sum of the individual responses [12]. When AC signal is introduced to the system, plotting potential vs time will give a sinusoidal curve. The potential will vary between negative and positive potentials with constant amplitude and the DC current will have a constant potential. This means that the sum of the curves will be a sinusoidal curve but it will not necessarily be symmetric across the x-axis.

In an electrochemistry point of view this means that the component to be protected in the circuit will change between being anode and cathode. It is expected that the component will undergo corrosion during the anodic half sine wave. Since the DC current from the sacrificial anode will polarize the steel in cathodic direction, the superimposed curve will have more negative potential than the single AC signal as is shown in Figure 2.3.
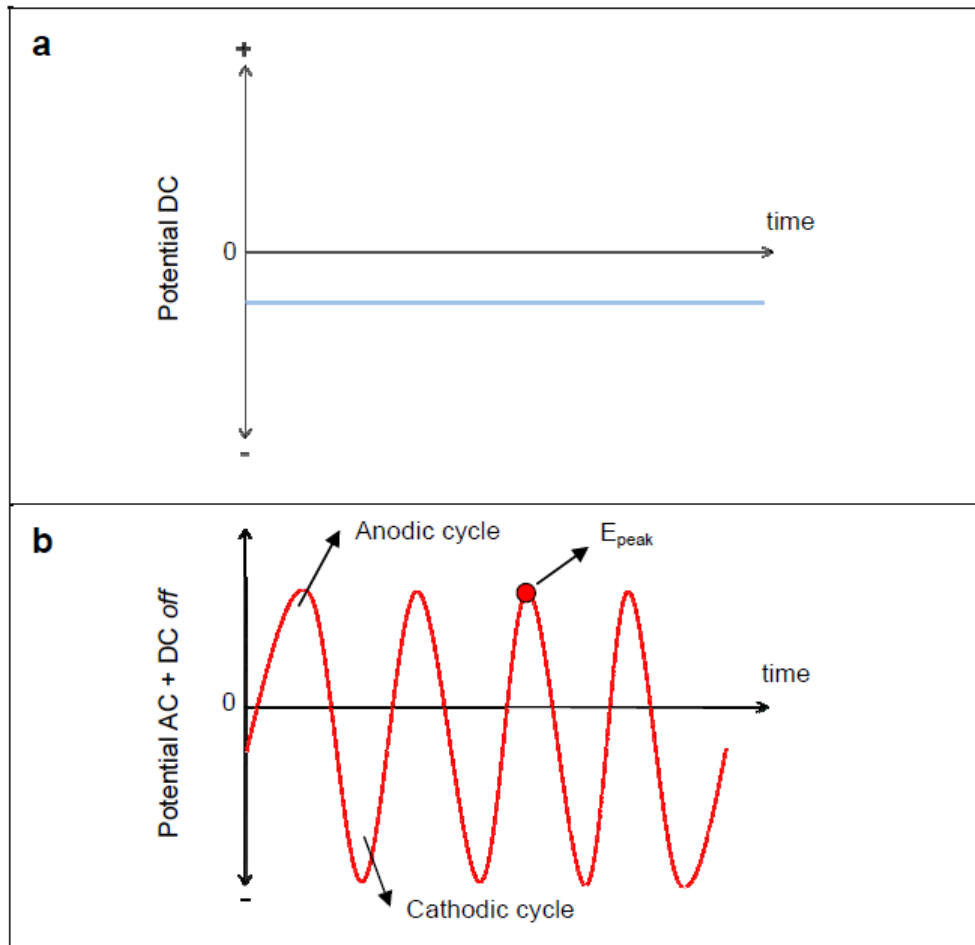
Figure 2.3: (a) DC potential at a cathodically protected steel without AC. (b) DC + AC potential at a cathodically protected steel with AC interference [13].

2.4 AC corrosion with cathodic protection

The effect of AC corrosion on cathodically protected steel is a subject that has received increased attention the last couple of years. However, there is still lack of knowledge about this and scientists do not agree on the cathodic protection properties when AC is applied to steel.

AC corrosion with CP was first investigated in the early 60's. A lot of scientists, including Bruckner, Hewes and Hamlin, reported that AC corrosion can be reduced to negligible values in the presence of cathodic protection. Tests have shown that the potential of the steel electrodes became more electropositive with increasing AC current density and the protection current density increased. The view that AC corrosion was insignificant when cathodic protection was applied was not supported by Devay. He performed tests where the corrosion rates were measured when an iron couple was subjected to AC current densities from 0 to 250 A/m^2 and DC current densities from 0 to 10 A/m^2. The results showed that although increased DC current densities reduced the corrosion, the corrosion rate was still significant. He also showed the depolarizing effects of AC on the anodic and cathodic polarization characteristics. Figure 2.4 shows that the potential will become more electropositive with increasing AC when carbon steel is polarized in cathodic direction [14].
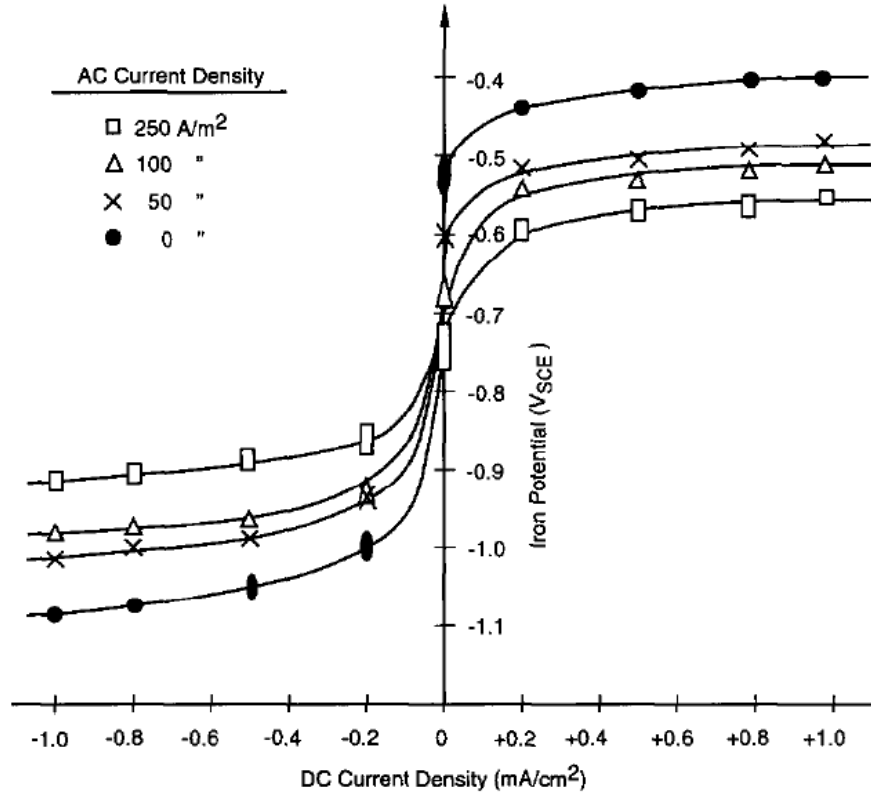
Figure 2.4: The effect of AC in polarization of steel [14]

AC corrosion was first identified in field in Germany in 1986 on a polyethylene coated gas pipeline under cathodic protection. The polarized protection potential due to cathodic protection was -1000 mV_{SCE} and the pH near the cathode was 10. This indicated that the CP was operating adequately with respect to the industry standards. A steel rod coupon was installed and monitored for a period of 220 days. Despite cathodic protection current densities of 1,5 to 2 A/m^2, the coupon experienced pitting corrosion. It was concluded that although protection current densities up to 10 A/m^2 reduced the corrosion rate, the resulting corrosion attack could not be reduced to negligible values. In the last couple of years, several cases of AC corrosion on cathodically protected steels have been identified over the whole world [14].

Today, most scientists agree that CP can be effective at "low" AC current densities, but not at "high" current densities. Below the threshold value of 20 A/m^2 of applied AC current on cathodically protected steel, corrosion is significantly reduced, while above 100 A/m^2 corrosion is expected [14, 15]. Yunovich et al. [16] supported this theory by performing tests with different polarization values and AC current densities. The results showed that at an AC current density of 20 A/m^2 and CP of 100-150 mV polarization decreased the corrosion rate compared to the control (no AC and no CP). However, at an AC current density of 500 A/m^2 and CP of 150-300 mV polarization, the corrosion rate actually increased compared to the control [14]. It has also been reported that for AC current densities of 20 A/m^2, the protective potential criteria usually used for cathodic protection does not apply [15].

Galsgaard and Nielsen [17] reported that the alkalization mechanism on the steel surface is one of the most important factors which have an impact on AC corrosion. Figure 2.5 shows the Pourbaix diagram for steel in water. When the pH at the steel surface increases, the steel might move into the active region to the right in the diagram. Such a high pH does not exist in any natural environment and must be created locally in a coating damage with cathodic protection. In this region, steel will corrode due to the reaction:

$$Fe + 2H_2O \rightarrow HFeO_2^- + 3H^+ + 2e^- \tag{2.10}$$
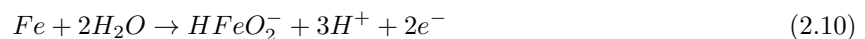
Traditional methods to prevent AC corrosion have been to add a surplus of sacrificial anodes and in cases reported with AC corrosion authors have stressed out that the CP system was operating well and the pH at the surface was high. According to Galsgaard and Nielsen, this strategy has been fatal. pH increase from cathodic protection in combination with vibrating potential from the AC current may lead to periodic entering the high pH corrosion area in the Pourbaix diagram. Galsgaard and Nielsen's work indicates that the corrosion rate may increase with higher CP current density.
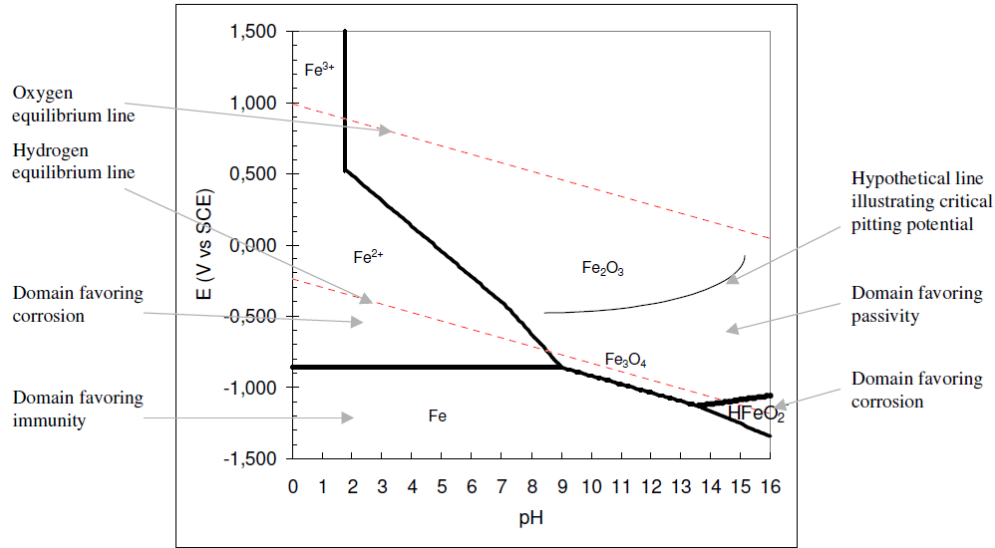
Figure 2.5: Pourbaix diagram for carbon steel in sea water [17].

Weight loss can be calculated by Faraday's law:

$$W = \frac{W_0}{nF} \int_0^t I_{ox} dt \qquad (2.11)$$

Where:

I = Current transfer

W_0= Molecular weight of corroded metal

n = Number of electrons transferred by the charge transfer reaction

F = Faraday's constant (96487 C/equiv.)

Corrosion rates can be calculated by the equation

$$CR = \frac{KW}{ATD} \qquad (2.12)$$

Where:

K = A constant $(8,76 \times 10^4$ for mm/year)

T = Time of exposure in hours

A = Area in cm^2

W = Mass loss in grams

D = Density in g/cm^3 (7,86 for carbon steel)

10

2.5 Effect of AC on calcareous deposits

Lilleby's studies [2] have shown that the AC current decreases with time for carbon steel under cathodic protection with a constant value of applied AC voltage (Fig. 2.6). She suggests that this is related to increased precipitation of calcareous deposits, which is supported by macroscopic observations of the film. In this work, the samples were polarized and the potential was held at a constant value of -1100 mV$_{SCE}$.
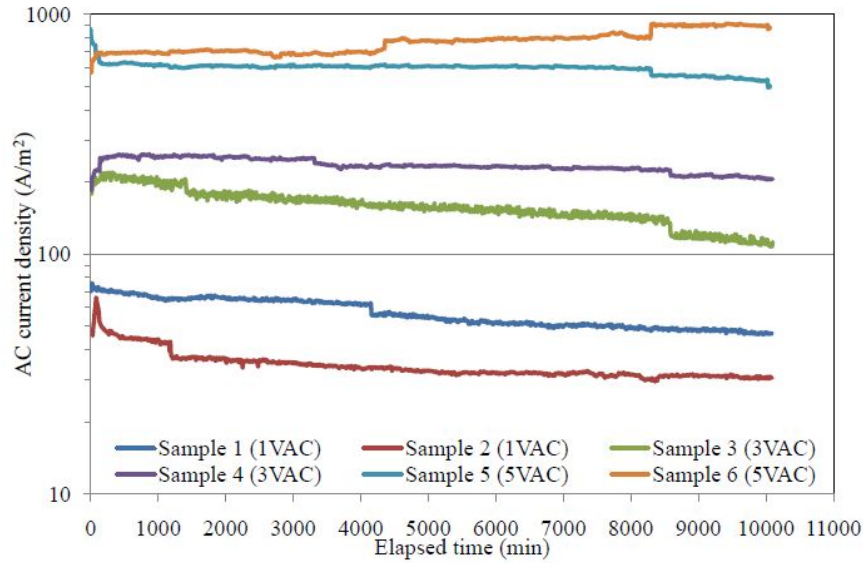

Figure 2.6: AC current vs time for cathodically protected steel with applied AC voltage

The changes in protection current density (Fig 2.7) in Lilleby's work were closely related to the AC current density. This indicates that the calcareous deposits formed during the exposure to AC voltage affected the DC current and AC current in a similar way. It can also be seen from the figure that the DC current density decreases for all samples which shows the protection properties of calcareous deposits.
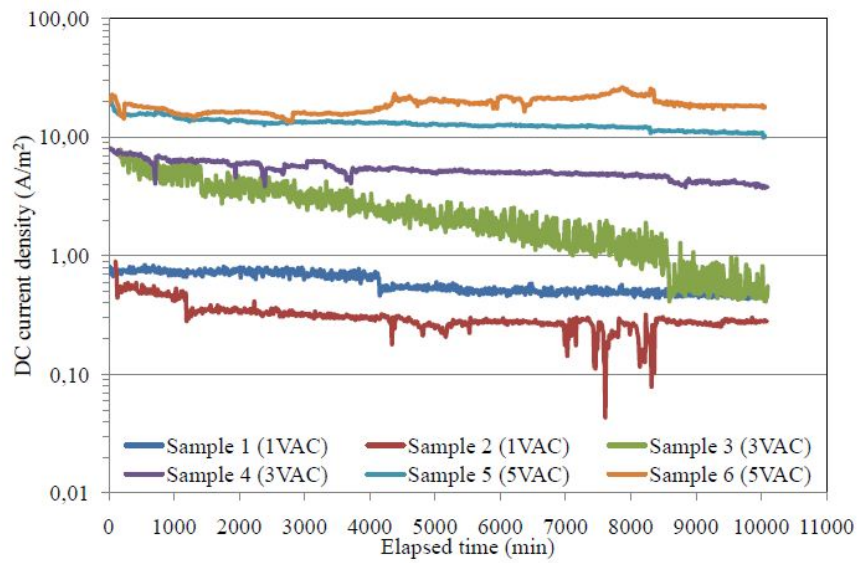

Figure 2.7: DC current vs time for cathodically protected steel with applied AC voltage

Investigations of the steel surface showed that white precipitate had formed on the edges of the deposits and at cracks in the deposits for the samples superimposed with AC. The precipitate was an Mg-rich phase and this indicates that an increase in pH at the cracks and edges allowed the Mg-rich phase to precipitate[18].

2.6 AlZnIn Sacrificial anode

Because of its economic advantage due to high theoretical current capacity and low active potential, Aluminum is well suitable for sacrificial anodes in offshore applications, although the formation of oxide gives a high passivation effect. Alloying elements are therefore used to shift the operating potential to more electronegative values and also produce a more uniform attack morphology. From commercially produced Al sacrificial anodes, there is today little doubt that AlZnIn anodes present the best performance in seawater. The average operating potential of AlZnIn anodes in this media has been reported to be -1,1 V_{SCE}. The attack morphology of this alloy shows hemispherical pits with a relatively smooth surface. This morphology was also obtained on an Al electrode activated in the presence of In^{3+} and Zn^{2+}.

There has been reported that the formation of $ZnAl_2O_4$ results in a higher instability of the Al oxide layer which can explain the role of Zn in the activation process. A small amount of Zn has an effect mainly on propagation and repassivation of metastable pits and not on their nucleation frequency[19]. In do also play a significant role in the activation of the AlZnIn anode due to segregation of In. The process can be classified in three steps (Fig. 2.8). (a) The In rich segregated phase, as a small anode, forms a galvanic cell with the Al_2O_5 film as a large cathode. The In rich segregated phase dissolves until the Al matrix is exposed to the electrolyte. (b) The Al matrix then forms a new high potential galvanic cell with the Al_2O_5 film. This results in active dissolution of the Al matrix and the In rich segregated phase becomes cathode and stops dissolving. (c) After the dissolution of the surrounding Aluminum, the In rich particles separate from the matrix and dissolve in the electrolyte [20].
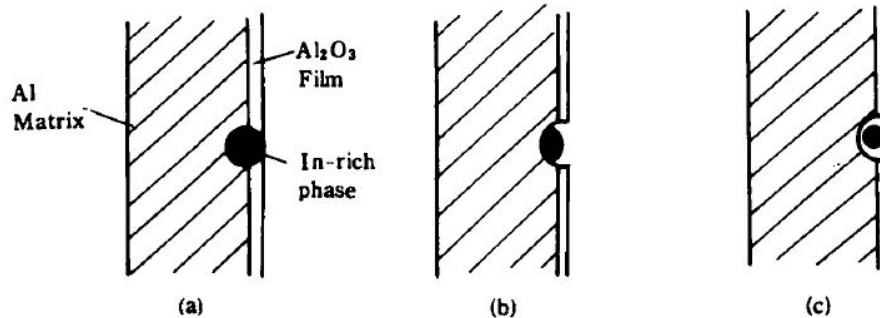

Figure 2.8: The activation process of Indium in AlZnIn sacrificial anode [20].

2.7 Aluminum exposed to alternating current

2.7.1 Corrosion mechanism

In recent years it has been increased focus on AC electrograining mechanisms and the parameters that affects the pitting morphology of Aluminum. The reason for this is the increased demand for high quality litho-printing and super capacitors for energy storage. Both applications need a controlled roughened surface which can be achieved from AC electrograining.

Oxidation of Aluminum occurs during the anodic half cycle and forms cubic pits at the surface. The reactions taking place are:

$$Al \rightarrow Al^{3+} + 3e^- \tag{2.13}$$

$$2H_2O \rightarrow O_2 + 4H^+ + 4e^- \tag{2.14}$$

During the cathodic half cycle, the following reactions occurs:

$$2H^+ + 2e^- \rightarrow H_2 \tag{2.15}$$

$$Al^{3+} + 3OH^- \rightarrow Al(OH)_3 \tag{2.16}$$

Due to reaction (2.15), the pH at the surface will increase and Aluminum hydroxide will precipitate at the surface as a white gel. This will form a protective film and increase the potential. The cathodic half cycle involves a repassivation of the surface resulting in a re-distribution of pits during the anodic half cycle. A schematic representation of this can be seen from Figure 2.9. Depending on the electrolyte and AC current density, the pitting morphology can vary between uniform, non-uniform and etch-like morphology.
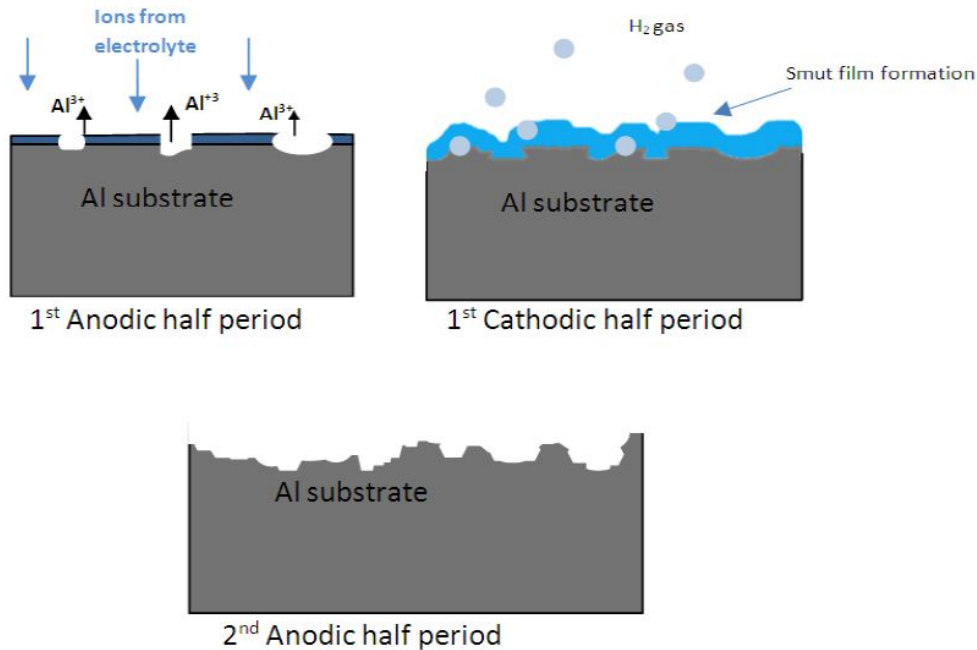
Figure 2.9: Pitting morphology on Aluminum exposed to AC [21]

When the current density is increased, the passive layer will become thicker because of the increased amount of Aluminum inside the pits during the anodic half wave and the pH increase during the cathodic half wave. This will result in decreased population density of pits which means that high current will give less but bigger pits [21].

Chapter 3

Experimental

3.1 Synthetic seawater

The synthetic seawater used in this work was prepared in accordance with ASTM D 1141. The composition of the seawater can be seen from Table 3.1

Table 3.1: Synthetic seawater in accordance to ASTM D 1141

Compound	Concentration [g/L]
NaCl	24,530
$MgCl_2$	5,200
Na_2SO_4	4,090
$CaCl_2$	1,160
KCl	0,695
$NaHCO_3$	0,201
KBr	0,101
H_3BO_3	0,027
$SrCl_2$	0,025
NaF	0,003

3.2 Material specification

The materials used in this work was Carbon steel (st52-3 U) and commercially Al-5Zn-0,02In sacrificial anode. The composition of the carbon steel can be seen from Table 3.2

Table 3.2: Composition of carbon steel

%C	%Mn	%Si	%S	%P
0,22	1,60	0,60	0,40	0,04

3.2.1   C-steel

The steel samples were machined to a rectangular shape with dimensions of $80mm \times 20mm \times 1mm$. All samples in this project work were grinded with SiC-paper to 1000 grit. Before the experiments, each sample was painted with Miccroshield to make an exposure area of 3,5 cm^2 as can be seen from Figure 3.1(a). Miccroshield is a painting with red color which is normally used in electrochemical applications. Each sample was weighted before painting. The painting free area to the right in the picture is the exposure area to the electrolyte. The sample has also an area free of painting in the other end to make electrical contact to the circuit.

3.2.2   AlZnIn

The AlZnIn samples were machined to 2 different shapes. One set of samples was machined to rectangular shape with dimensions of $80mm \times 20mm \times 3mm$. These samples were painted with Miccroshield which gave an exposure area of $8cm^2$. The other set were sacrificial anodes and these samples had also a rectangular shape with dimensions of $60mm \times 30mm \times 5mm$. To obtain and area ratio of 1:10 between anode and cathode, these samples were painted with Miccroshield which gave an exposure area of 35 cm^2 (Fig 3.1 (b)). Each sample was weighted before painting.
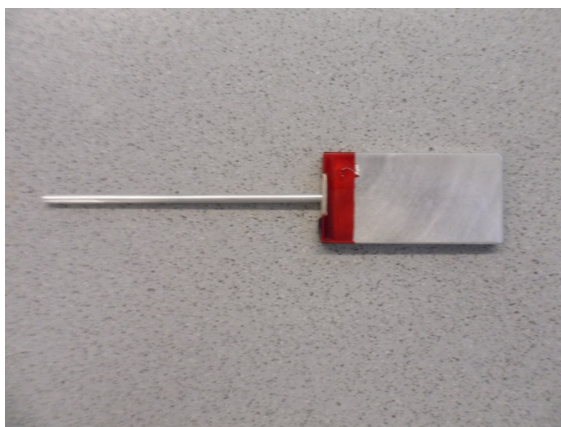
    (a) Carbon steel   **(b)** AlZnIn sacrificial anode

Figure 3.1: Painted samples for the experiments

3.3 Reference electrode and salt bridge

The reference electrode used in this work was a saturated calomel electrode (SCE). SCE consists of metallic mercury in contact with calomel or mercury(1) chloride (Hg_2Cl_2), which is in contact with KCl. The electrode reactions are:

$$Hg_2Cl_2(s) + 2e^- \rightleftharpoons 2Hg(l) + 2Cl^-(aq) \tag{3.1}$$
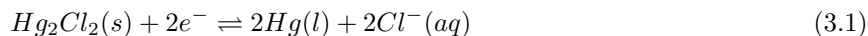
All potentials in this report is in reference to the SCE. A salt bridge was used to attain ionic contact between the reference electrode and samples. The salt bridge consisted of saturated KCl and agar solution.

3.4 Apparatus

3.4.1 Formation of calcareous deposits

Six samples were placed in a vessel filled with synthetic seawater and an AlZnIn sacrificial anode. The anode was connected to the samples through a 1Ω-resistor. An Agilent 34970A data logger was used to measure the potential of the steel samples, the resistance and the potential drop through the resistor for each sample every hour. Figure 3.2 shows a drawing of the circuit while the test setup can be seen from Figure 3.3.
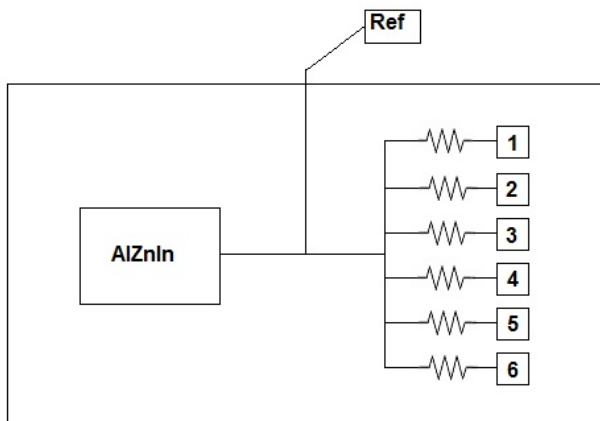
Figure 3.2: Electrical circuit diagram of the formation of calcareous deposits experiment
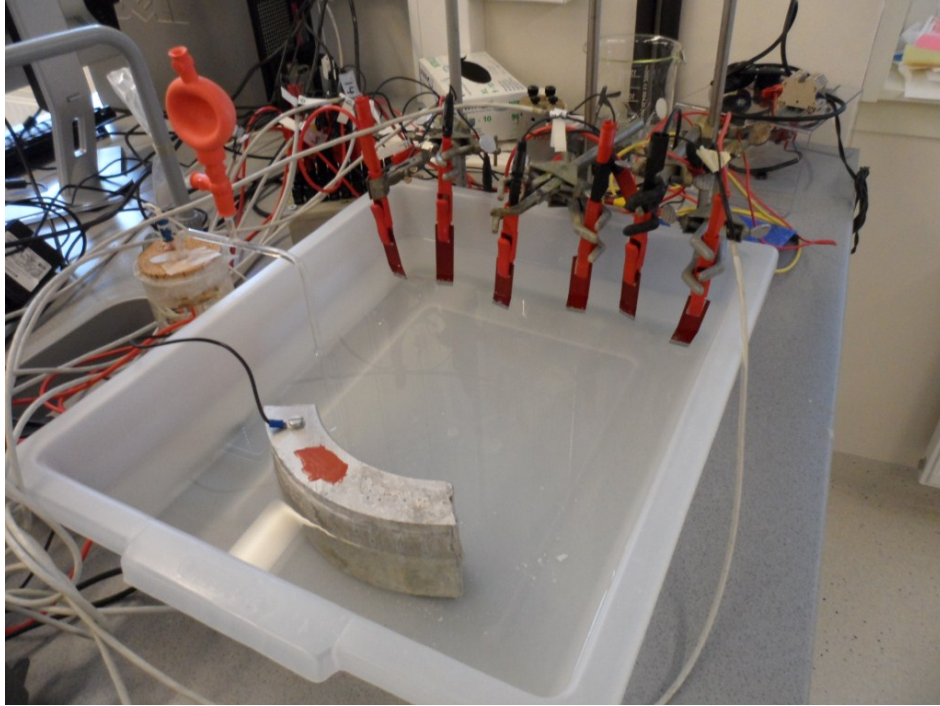
Figure 3.3: Test setup for the formation of calcareous deposits experiment

3.4.2 Cathodic protection with superimposed AC

After the pre exposure, each steel sample was placed one by one in a vessel filled with synthetic seawater and a sacrificial anode as described in section 3.2.2. The sacrificial anode was connected to a 10 H inductor and a 1Ω-resistor to measure the DC current density. A VariAC and a 500 µF Capacitor was connected in parallel to superimpose AC current and to prevent DC current to flow into the AC circuit. The Agilent 34970A data logger was used to measure the DC current density, AC current density and DC potential every 30 minutes during the exposure time. Fig 3.4 shows the circuit diagram and Fig 3.5 shows a picture of the setup.
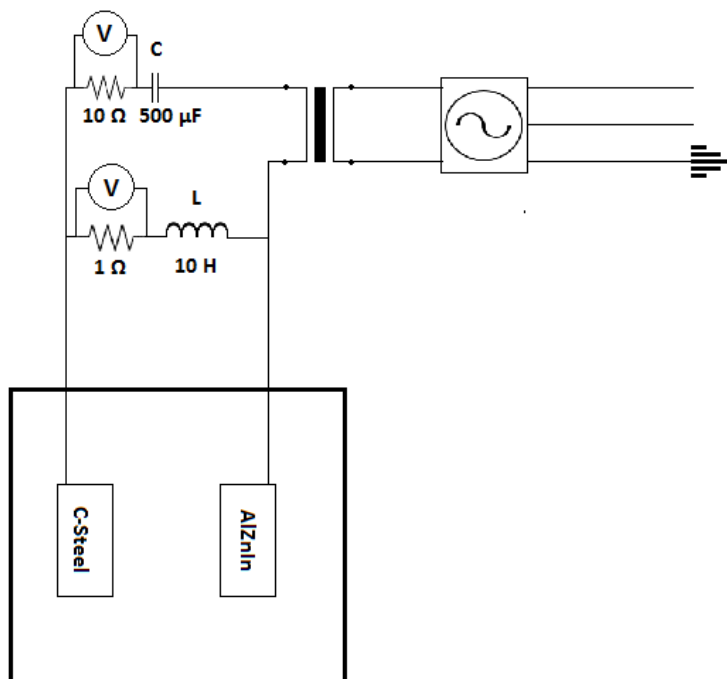
Figure 3.4: Electric circuit for the CP with superimposed AC experiment.
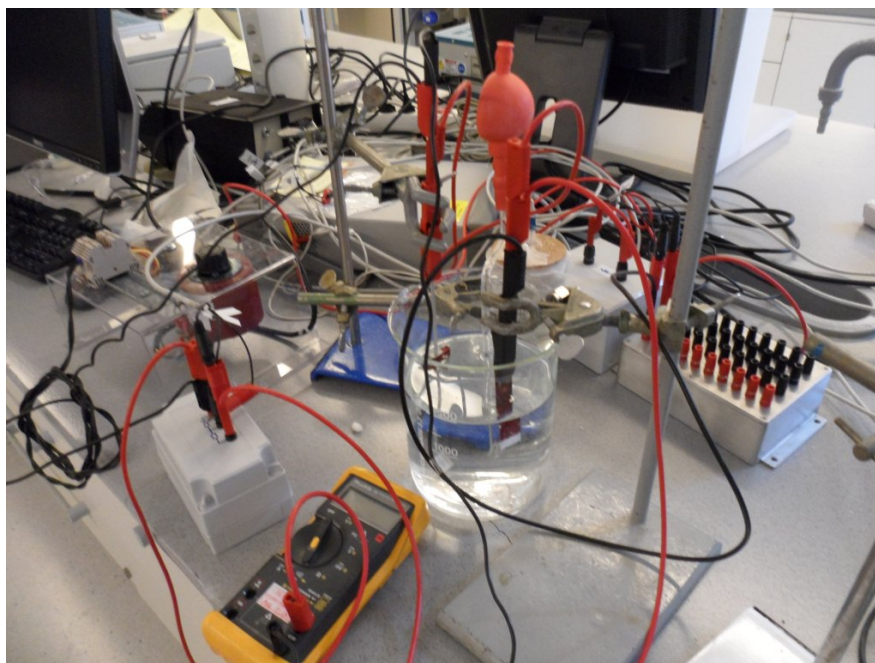
Figure 3.5: Setup for the CP with AC experiment.

3.4.3 Polarization curves

A total of 6 samples, one at a time were placed in a vessel filled with synthetic seawater and two titanium counter electrodes. There were one AC circuit and one DC circuit in the setup. The setup contained a 500 µF capacitor to separate the DC current from the AC circuit. An 10 L inductor was also connected to separate the AC current from the DC circuit. The AC current was measured through a 10Ω-resistor and the circuit can be seen from Fig 3.6. A Gamry framework potentiostat, version 5,50 was used to polarize the samples and measure the DC current.
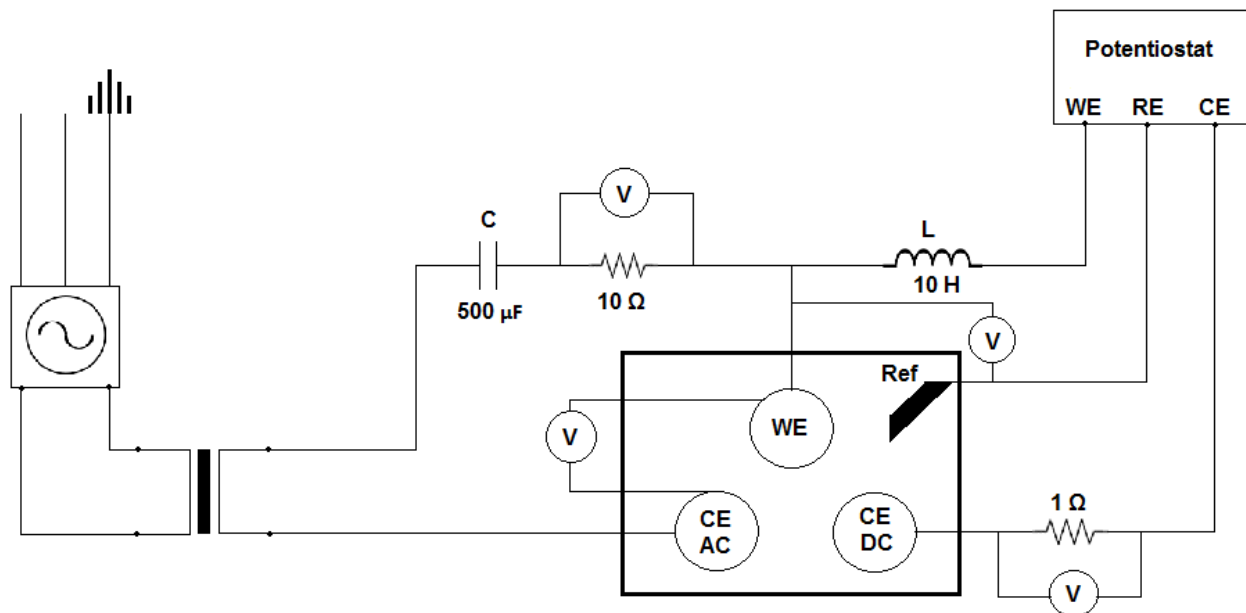
Figure 3.6: Circuit diagram for the polarization curve experiment

3.4.4 Potential measurement of AlZnIn

The samples used in this experiment were the same samples as those used in the polarization curve experiment described in section 3.2.2. Two samples with an area of 9,8 cm^2 were placed in two separate test setups. The setup was the same as the polarization curve setup described in section 3.4.3 but the Gamry potentiostat was not used in this experiment. An Agilent 34970A data logger was used to measure the potential of the samples.

3.5 Test procedure

3.5.1 Formation of calcareous deposits

The samples were exposed to synthetic seawater, under cathodic protection by the sacrificial AlZnIn anode for three weeks. The electrolyte was held at room temperature during the whole test period and the water

level was controlled by adding distilled water when the level dropped. After three weeks, the samples were removed from the setup, air dried and stored for the AC experiment. Macroscopic pictures were taken of the samples.

3.5.2   Cathodic protection with superimposed AC

The samples were separately exposed to synthetic seawater under cathodic protection and applied AC voltage for one week. All samples were exposed to the electrolyte for 30 minutes with superimposed AC voltage before the experiment started. The AC voltages were respectively 0 V (Sample 1), 1 V (Sample 2), 2 V (Sample 3), 3 V (Sample 4), 4 V (Sample 5) and 5 V (Sample 6). In this report, the different samples will be referred to the terms written in the parentheses. The electrolyte was held at room temperature during the test period. After one week, the samples were removed from the experiment, macroscopically photographed, cleaned in accordance to ASTM G1-03 and weighted. They were then stored for further investigations in SEM.

3.5.3   Weight loss measurement

The weight loss procedure was done in accordance to ASTM G1-03. For carbon steel the cleaning solution was 500 ml HCl, 3.5 g hexamethylene tetramine and 500 ml distilled water. The samples were exposed to the solutions in cycles that lasted for 10 minutes at room temperature. In the case of the AlZnIn samples, the cleaning solution was 50 mL phosphoric acid, 20 g chromium trioxide and 950 ml distilled water. Each cycle lasted for 5 minutes and the temperature was 90-100ºC. The samples were weighted between each cycle for both AlZnIn and carbon steel. Before the experiments started, a carbon steel sample and a AlZnIn sample were undergone the same cleaning procedures to correct for etching of base metal.

3.5.4   SEM characterization

All samples that were involved in the experiments with CP, both steel and AlZnIn, were studied in FESEM, Zeiss Ultra 55 Limited edition after the experiments. The working distance was 6 mm and the electron acceleration voltage was 5,00 KeV. For each AlZnIn sample, one overview picture was taken at 25 X Magnification followed by a more detailed picture at higher magnification. In the case of the steel sample one picture was taken of one of the samples. The reason for this was that all the surfaces for the different steel samples were equal.

3.5.5   Polarization curves

The samples were exposed to the electrolyte at open circuit potential at 5 minutes without AC and 3 minutes with AC before the potential sweep started. For the sample without AC, the exposure time was 8 minutes at open circuit potential without AC. This was due to stabilization of the potential to get equal conditions before the test. Different values of AC current densities were applied to the samples as can be seen from Table 3.3. The potential sweep was in anodic direction for all the samples. Table 3.3 shows the initial and final potential for each sample.

Table 3.3: Initial and final polarization potential for the samples

Sample	AC current density $[A/m^2]$	Initial potential [V]	Final potential [V]
1	0	-1,40	-0,60
2	50	-1,50	-0,70
3	100	-1,50	-0,70
4	150	-1,60	-0,80
5	200	-1,60	-0,80
6	250	-1,60	-0,80

3.5.6 Potential measurement

The two AlZnIn samples were exposed to synthetic seawater with applied AC current densities of respectively 100 A/m^2 and 200 A/m^2 for 72 hours. The potential of each sample was logged every 15 minutes and the logger started to log data immediately after the sample were placed in the setup. The electrolyte was held at room temperature and the water level was controlled by adding distilled water to the electrolyte.

Chapter 4

Results

The results presented in this chapter is based on comparison of the different experiments. Single curves for each experiment can be seen in the Appendix.

4.1 Formation of calcareous deposits

Figure 4.1 shows a macroscopic picture of one of the samples pre exposed to cathodic protection. It can be seen from the picture that the painting is still intact and calcareous deposits have formed uniformly at the surface, despite a small crack that can be seen at the center of the exposure area.

Figure 4.1: Calcareous deposits on carbon steel

Corrosion at the free exposed area that was not in contact with the electrolyte could be seen on all samples. This area was located above the water level which means that it was not under cathodic protection.

Figure 4.2 shows the potentials and Figure 4.3 shows the current densities of the steel samples during the exposure time of 504 hours. The potential is quite unstable during the first 300 hours. After 300 hours, the potential increases significantly to -0,30 V. At this stage, the reference electrode was replaced by a new reference electrode and the potential dropped to -1,05 V. This was also the potential for the remaining exposure time. It is believed that the first reference electrode did not operating well and the dotted line represent the probable potential during the whole experiment. The potential during the first 300 hours should therefore be ignored. Each sample showed identical potential during the whole exposure time.
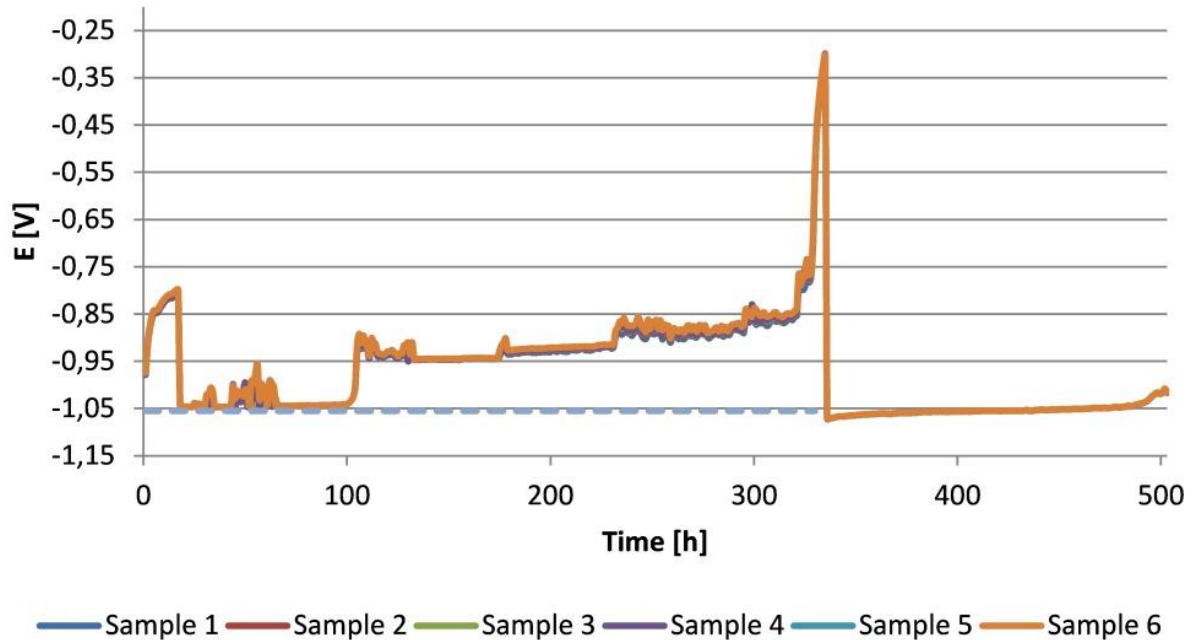
Figure 4.2: Potentials on the samples during the pre exposure

The current density decreased for all the samples during the pre exposure. The reduction rate was highest during the first 100 hours for all the samples followed by a relatively constant value for the last 400 hours. The reduction rate and current density were lower at the early stages of the experiment for sample 1 and 5 compared to the other samples.
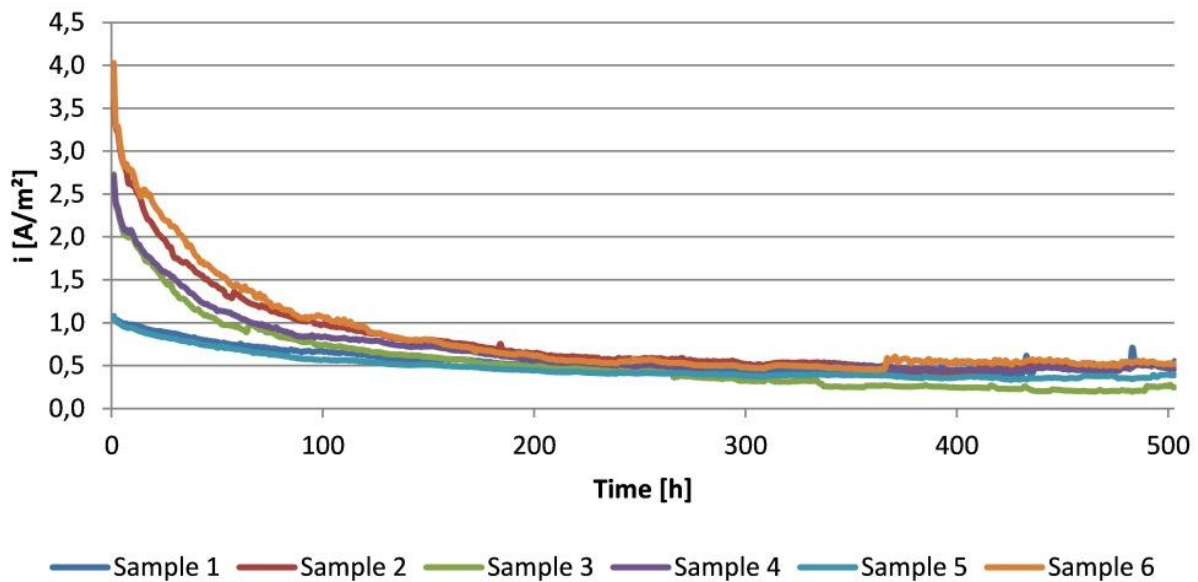
Figure 4.3: Current densities on the samples during the pre exposure

Table 4.1 shows the initial and final current densities for each sample. There is a large variation in initial

current density, varying between 1,1 and 4,1 A/m^2. The final current density is quite stable for all samples, varying between 0,4 and 0,6 A/m^2, except sample 2 which has a final current density of 0,2 A/m^2.

Table 4.1: Initial and final current densities for the pre exposure experiment

Sample	Initial current density [A/m^2]	Final current density [A/m^2]
1	1,1	0,6
2	3,6	0,5
3	2,7	0,2
4	2,7	0,5
5	1,1	0,4
6	4,0	0,5

4.2 Cathodic protection with superimposed AC voltage

Macroscopic pictures of the steel samples after the CP experiment with superimposed AC can be seen in Figure 4.4. The AlZnIn samples that have undergone the removal of corrosion products procedure in the same experiment can be seen in Figure 4.6. The calcareous deposits were still intact for all steel samples after the experiment. A non-uniform morphology in the layer can be seen at sample 2, 4 and 6 while the surface morphology is smoother for the other samples. Calcareous deposits can also be seen at the painting above the exposure area, following the bubble direction. The painting was still intact after the experiment.

The sacrificial anodes immediately after the experiments are shown in Figure 4.5. A white layer can be seen on all samples. For the samples exposed to 0, 1 and 2 V AC, this layer is in general presented in the corroded areas and it follows the direction of the hydrogen bubbles upward the sample. For the sample exposed to 3 V AC, the layer is presented at almost the entire surface and a large amount at the corroded area at the edge of the sample. The samples exposed to 4 and 5 V AC are both fully covered by this layer and it is thicker than for the other samples.

Macroscopic pictures of the AlZnIn samples after removal of corrosion products can be seen from Figure 4.6. The surface of the three samples with lowest AC value are characterized by large corroded areas surrounded by smooth surface. On sample 2 there is a band in longitudinal direction in the middle of the sample with small pits. Outside this areas, close to the edges of the sample on each side, the morphology is almost the same as for sample 1 and 3. That means large corroded areas surrounded by a smooth surface. Sample 4 had a large corroded area at one of the edges of the sample while there were small pits on the rest of the surface. The samples exposed to 4 V and 5 V AC had no such large corroded areas that could be seen at the other samples. On these two samples there were a uniform distribution of pits at the entire surface.
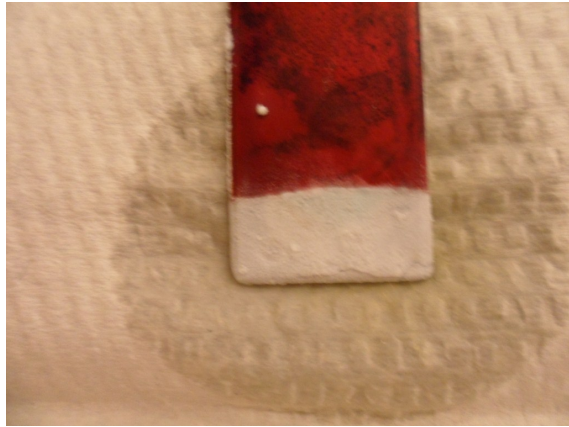
(a) 0 V AC
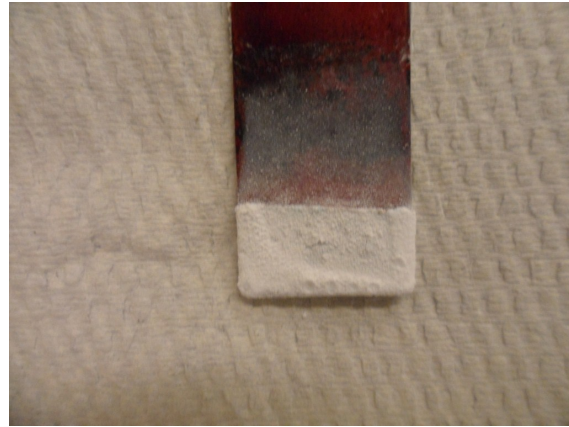
(b) 1 V AC
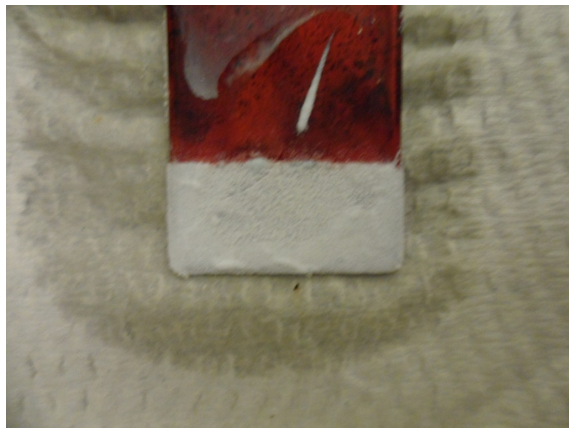
(c) 2 V AC

(d) 3 V AC

(e) 4 V AC

(f) 5 V AC

Figure 4.4: Pictures of steel samples under cathodic protection immediately after the experiment.

(a) 0 V AC

(b) 1 V AC

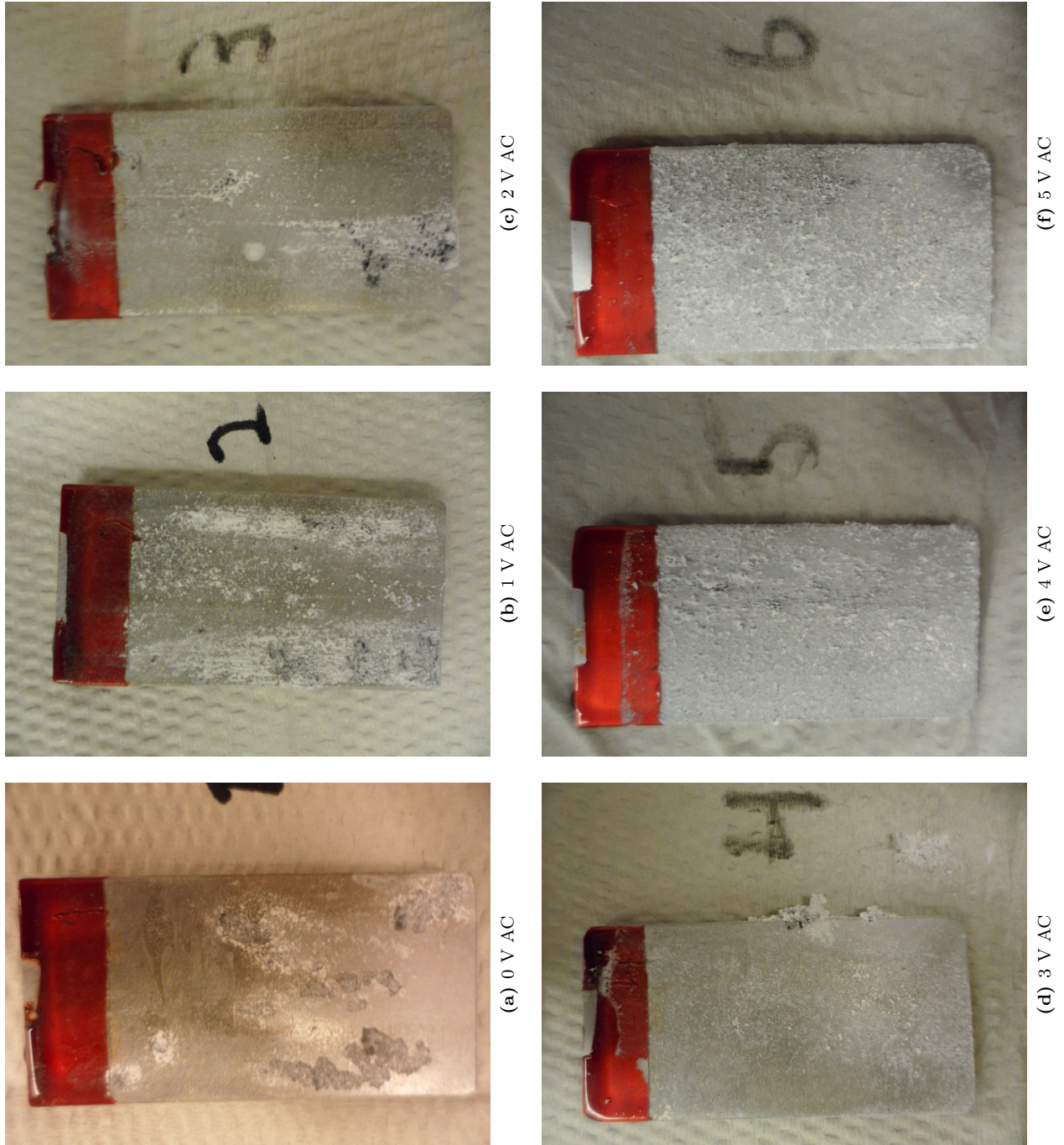(c) 2 V AC

(d) 3 V AC

(e) 4 V AC

(f) 5 V AC

Figure 4.5: Pictures of AlZnIn samples under cathodic protection immediately after the experiment.

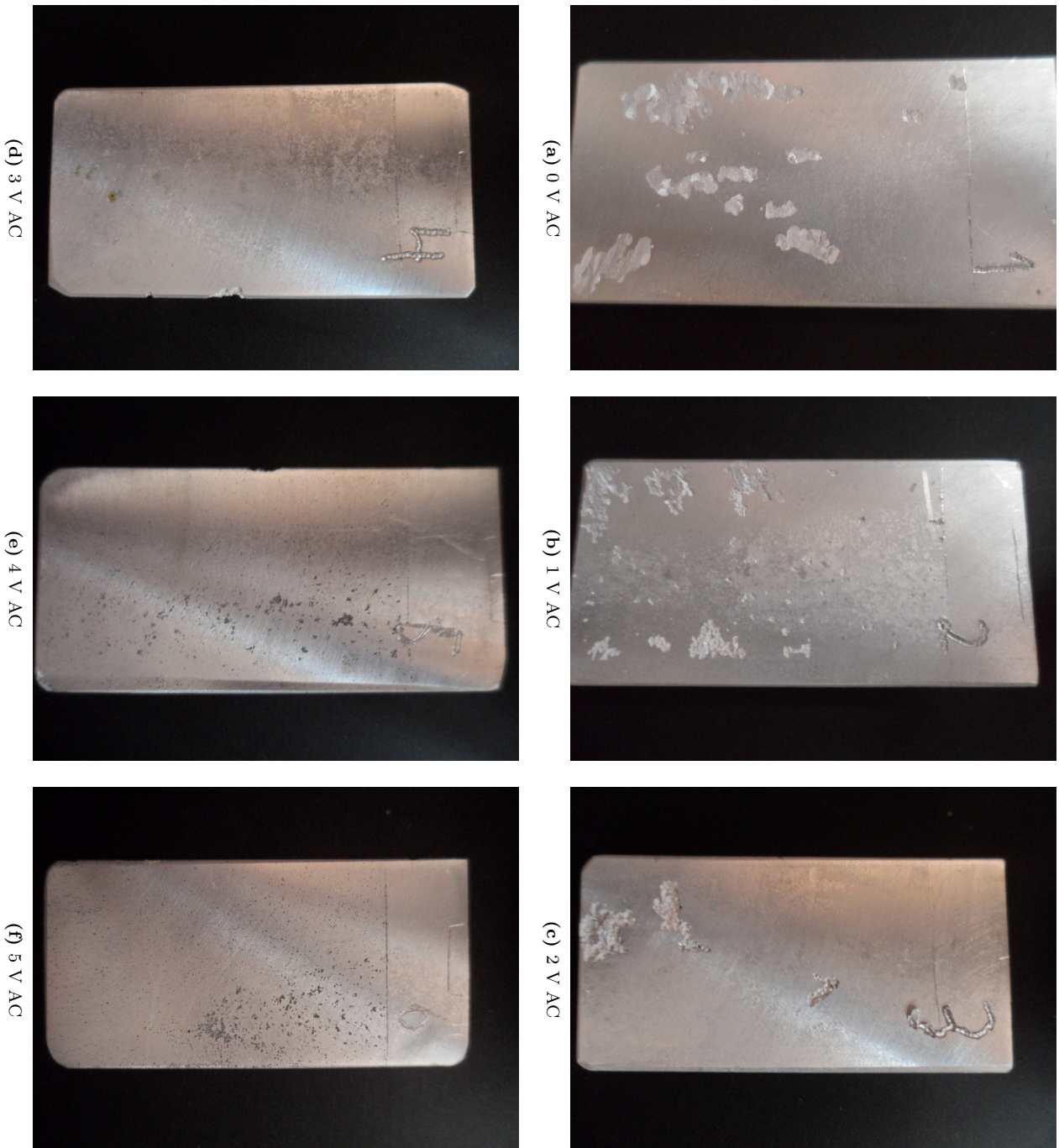**Figure 4.6:** Pictures of AlZnIn samples under cathodic protection with different AC values after removal of corrosion products

Figure 4.7 shows the potentials of the different samples during the exposure time. Sample 6 showed a rapid increase in potential during the first couple of hours to about -1,03 V and had the highest potential during the experiment. The potential of sample 5 varied between -1,04 and -1,06 V. An increase in potential from -1,16 V to -1,10 V can be seen for sample 4 during the first 40 hours. After this, the potential decreased slightly to about -1,13 V during the rest of the experiment. The potential of sample 1 decreased from -1,10 V to -1,12 V in the early stages of the experiment and flattened out at -1,12 V during the rest of the exposure time. Sample 3 had a potential of about -1,15 V the first 110 hours followed by a decrease to -1,14 V which lasted for the remaining exposure time. The lowest potential in this experiment was the potential of sample 2 which decreased from -1,15 V to -1,18 V during the first 50 hours followed by a slightly increase to -1,17 during the remaining exposure time. The potentials of the samples exposed to AC increased with increasing AC voltage.
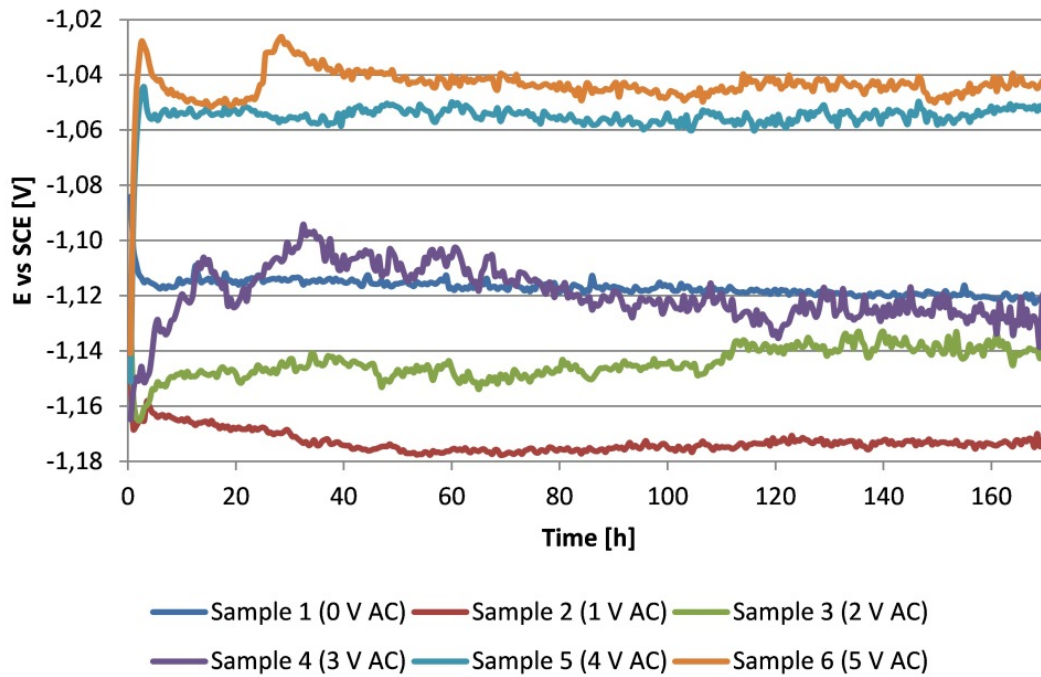
Figure 4.7: Potential vs time curve for the samples exposed to CP with applied AC voltage

The AC current density for the steel samples can be seen from Figure 4.8. For all samples, the AC current density increased with increasing AC voltage. Sample 2 and sample 3 had quite stable alternating current densities, respectively 30 A/m^2 and 150 A/m^2 during the whole exposure time. The AC current density of sample 4 varied between 300 A/m^2 and 500 A/m^2 while sample 5 had an AC current density varying between 700 A/m^2 and 2000 A/m^2. The sample with highest alternating current density in this experiment was sample 6 which had a current density varying between 800 A/m^2 and 2500 A/m^2. Figure 4.9 shows the AC current density values for the AlZnIn samples which is one tenth of the steel values due to the area ratio of 1:10.
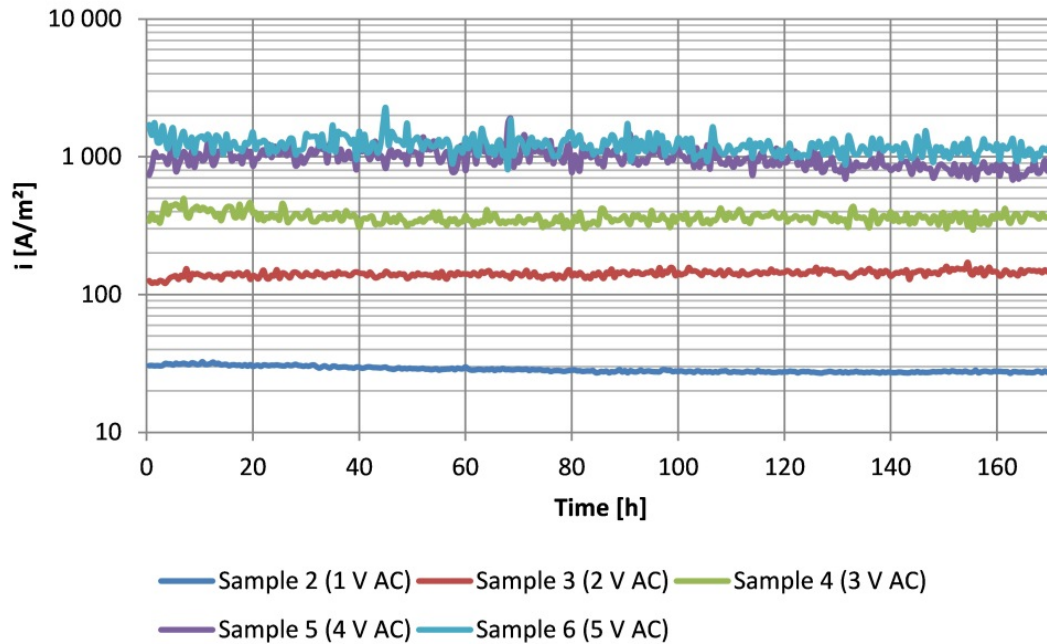
Figure 4.8: AC current density vs time for the steel samples exposed to CP with applied AC.
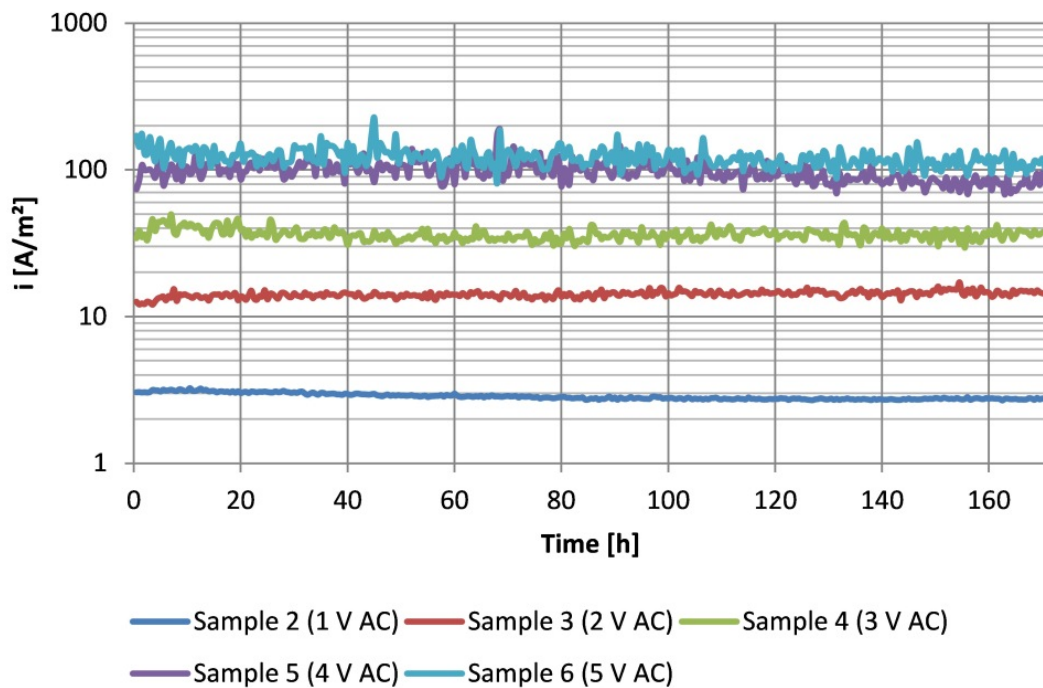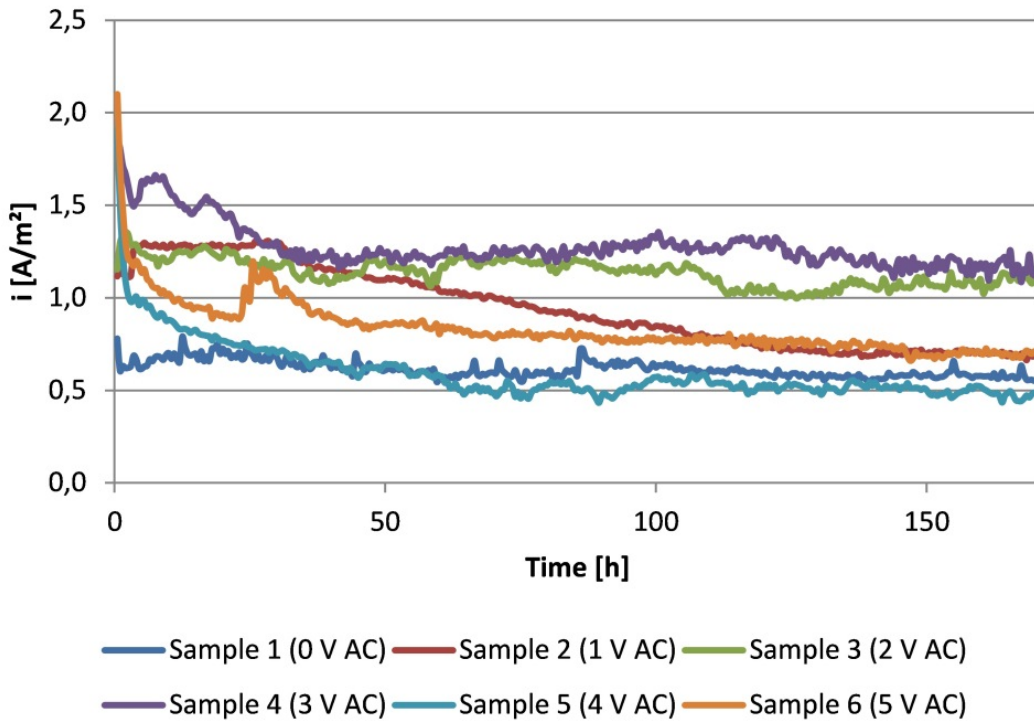

Figure 4.9: AC current density vs time for the AlZnIn samples exposed to CP with applied AC.

Figure 4.10 shows the DC current density for the steel samples during the exposure time. Sample 1 had a relatively constant value of DC current density in the order of 0,6 - 0,7 A/m^2. The DC current density of sample 2 decreased slightly from about 1,3 A/m^2 to about 0,7 A/m^2 during the first 120 hours of the experiment. The value was constant at 0,7 A/m^2 the rest of the exposure time. For sample 3, the DC value

varied between 1 A/m^2 and 1,4 A/m^2. Sample 4 had the highest average DC value of all samples in this experiment, starting at 1,9 A/m^2 followed by a decrease to about 1,3 A/m^2 after 40 hours. This DC value lasted for the remaining exposure time for sample 4. Both sample 5 and sample 6 showed a rapid decrease in DC current during the first couple of hours, from respectively 1,9 A/m^2 to 1,0 A/m^2 and 2,1 A/m^2 to 1,2 A/m^2. For sample 5, this was followed by a slightly decrease in DC current the next 60 hours to about 0,5 A/m^2 which was the value for the remaining exposure time. The DC value of sample 6 decreased to about 0,8 A/m^2 during the first 20 hours. This was followed by a rapid decrease to 1,25 A/m^2 before the curve decreased slightly to 0,7 A/m^2 during the last period of the experiment. Also in this case, the DC values of the AlZnIn samples was one tenth of the steel values because of the area ratio as can be seen in Figure 4.11.

Figure 4.10: DC current density vs time for the steel samples exposed to CP with applied AC
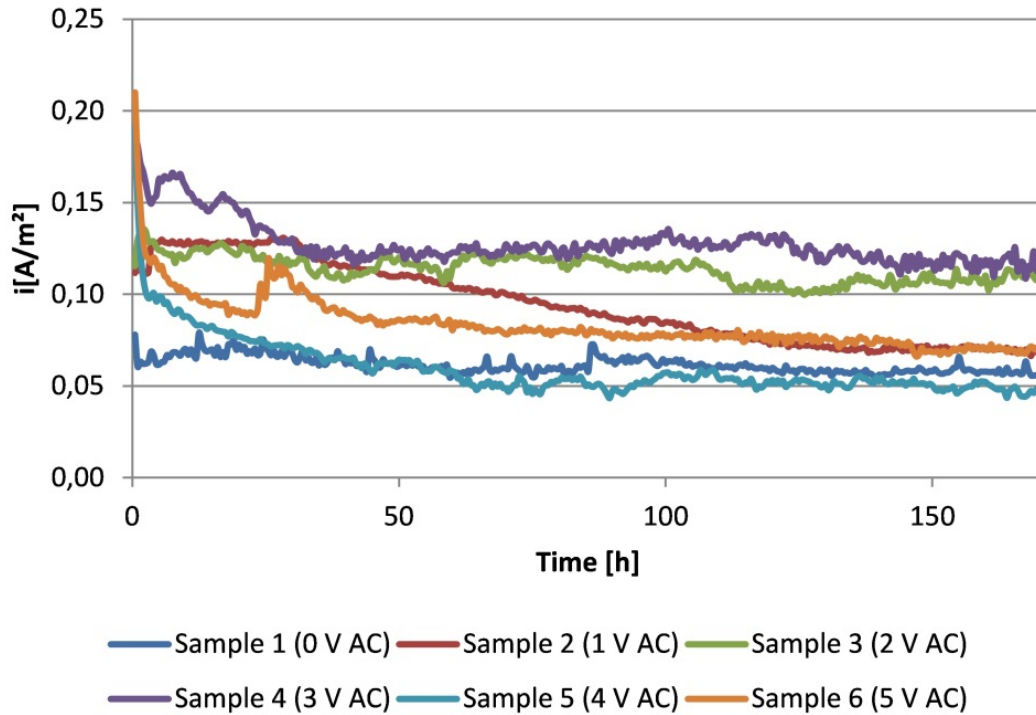
Figure 4.11: DC current density vs time for the AlZnIn samples exposed to CP with applied AC

Table 4.2 shows the corrosion rates on the steel and AlZnIn samples at different AC voltage values based on the weight loss measurements.

Table 4.2: Corrosion rates on the steel and AlZnIn samples

	0 V AC	1 V AC	2 V AC	3 V AC	4 V AC	5 V AC
Steel [mm/y]	0,073	0,058	0,068	0,056	0,063	0,097
AlZnIn [mm/y]	0,19	0,44	0,41	0,55	0,33	0,28

The corrosion rates as a function of AC current density can be seen from Figure 4.12. For the steel samples, the corrosion rates are relatively constant for AC current density below 1000 A/m^2. Above this value, the corrosion rate increases to 0,097 mm/year at an AC current density of 1200 A/m^2. A rapid increase in corrosion rate for AlZnIn occurs when AC is present. This is followed by a more slightly increase, reaching a peak at 0,55 mm/year at 400 A/m^2. The corrosion rate decreases with a constant rate for AC current densities above 400 A/m^2.
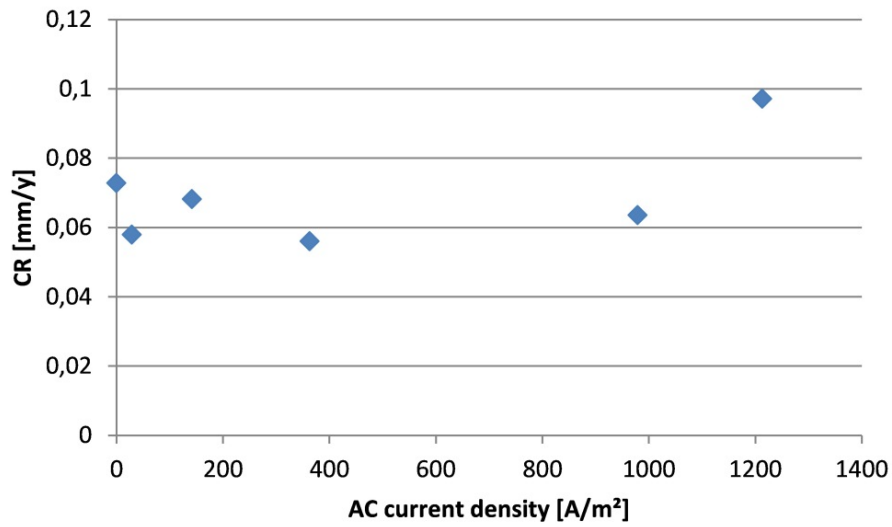
(a) Carbon steel
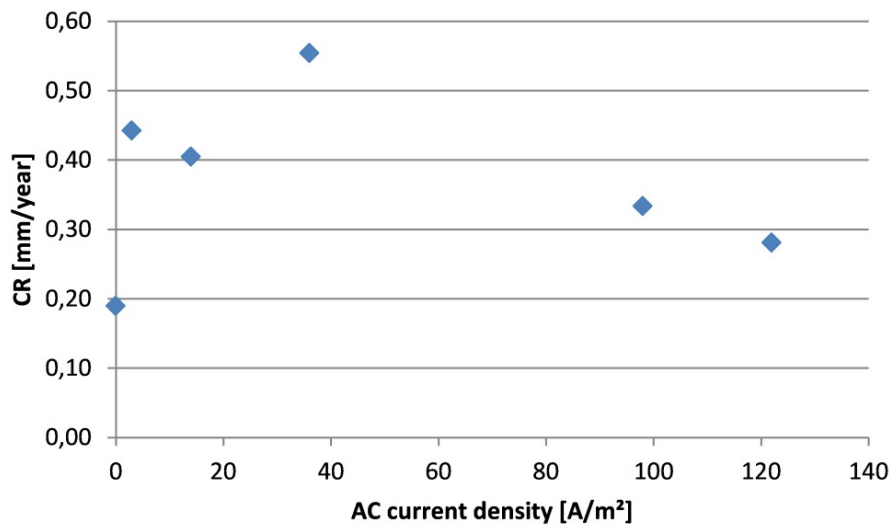
(b) AlZnIn

Figure 4.12: Corrosion rate vs AC current density for the CP experiment

Weight loss of the sacrificial anodes by self corrosion was calculated by integrating eq. (2.11). The contribution to the total corrosion rate of AlZnIn by self corrosion and protection of the steel samples can be seen from Table 4.3 and Figure 4.13.

Table 4.3: Corrosion rates of AlZnIn by self corrosion and protection of steel

V_{AC}	CR_{Tot} [mm/y]	$CR_{Self-corrosion}$[mm/y]	$CR_{Protection}$[mm/y]
0	0,19	0,00	0,19
1	0,44	0,16	0,28
2	0,41	0,06	0,35
3	0,55	0,17	0,38
4	0,33	0,15	0,18
5	0,28	0,03	0,25
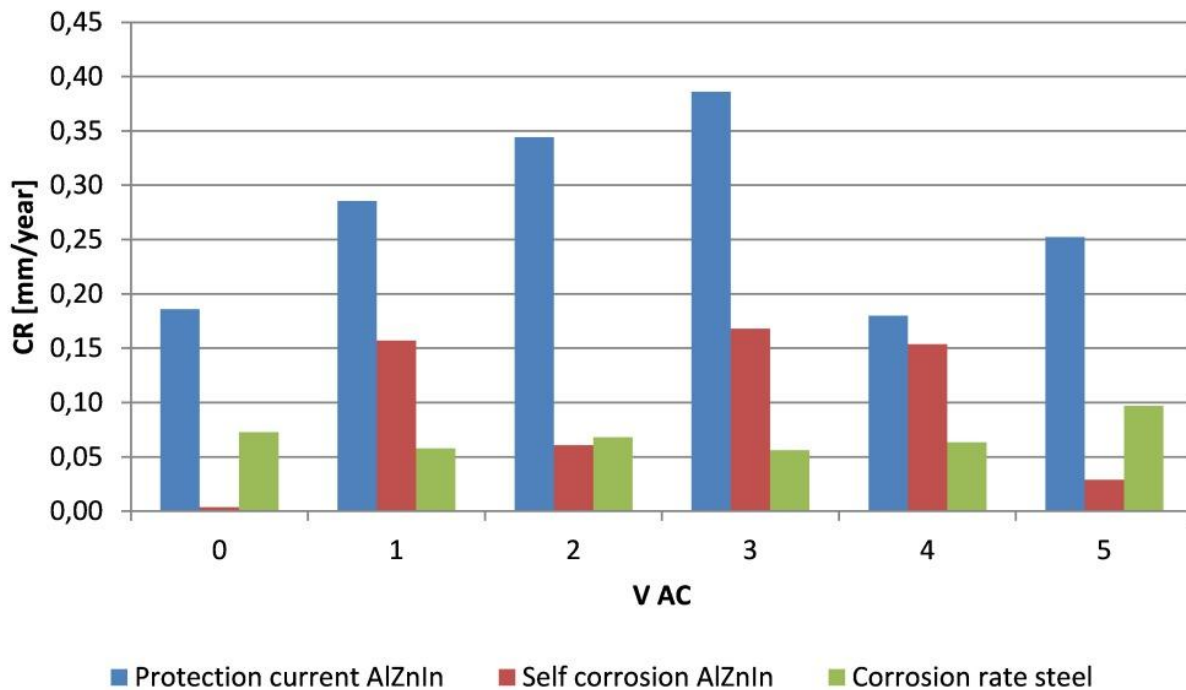
Figure 4.13: Corrosion rates of steel and AlZnIn by self corrosion and protection of steel.

The corrosion rate of AlZnIn due to protection of steel increases with increasing AC voltage up to 3 V AC. This is followed by a large drop in corrosion rate from 3 to 4 V AC. The corrosion rate of the sample exposed to 5 V AC is higher than the sample with 4 V AC, but still lower than the samples exposed to 1, 2 and 3 V AC. The sample without AC showed no self corrosion. For the other samples, the self corrosion rate is stable at 0,15 - 0,17 mm/year for the samples exposed to 1, 3 and 4 V AC. A relatively low value of self corrosion rate can be seen at the samples exposed to 2 and 5 V AC, respectively 0,06 and 0,03 mm/year.

A summary of average current densities, average potential and corrosion rate for each sample can be seen in table 4.4.

Table 4.4: Summary of the CP with applied AC experiment

	AC Voltage [V]	Average E vs SCE [V]	Average i_{AC} [A/m^2]	Average i_{DC} [A/m^2]	Corrosion rate [mm/year]
Steel	0	-1,12	-	0,62	0,073
	1	-1,17	29	0,94	0,058
	2	-1,14	142	1,14	0,068
	3	-1,12	363	1,28	0,056
	4	-1,06	979	0,59	0,063
	5	-1,04	1213	0,83	0,097
AlZnIn	0	-1,12	-	0,06	0,19
	1	-1,17	3	0.09	0,44
	2	-1,14	14	0,11	0,41
	3	-1,12	36	0,13	0,55
	4	-1,06	98	0,06	0,33
	5	-1,04	122	0,08	0,28

4.3 SEM Characterization

Microscopic pictures of the sample without AC voltage can be seen from Figure 4.14. Figure 4.14 (a) shows a large corroded area on the surface while Figure 4.14 (b) shows an enlarged picture inside this area. The area is characterized by peaks and valleys
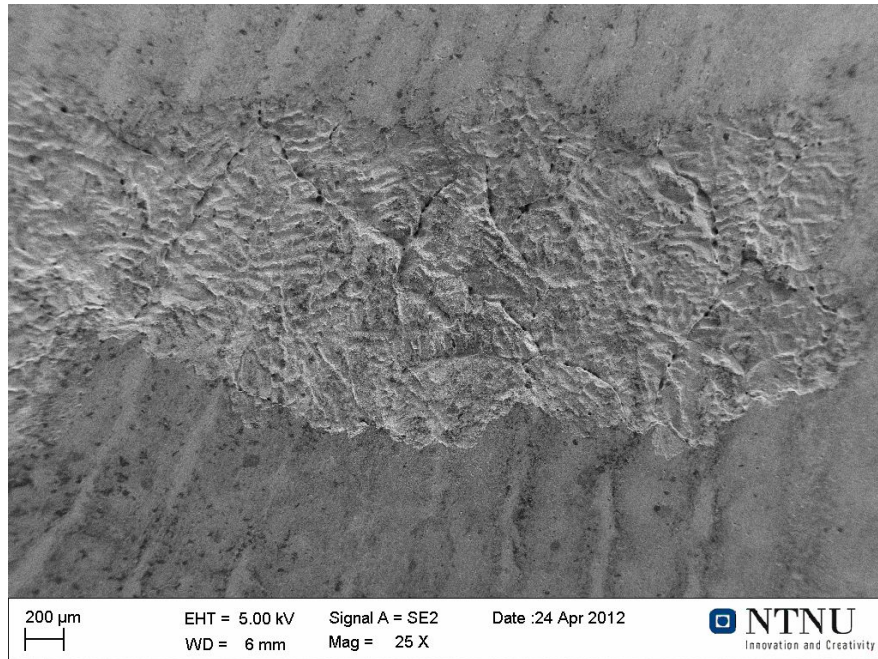
(a) 25 X Magnification
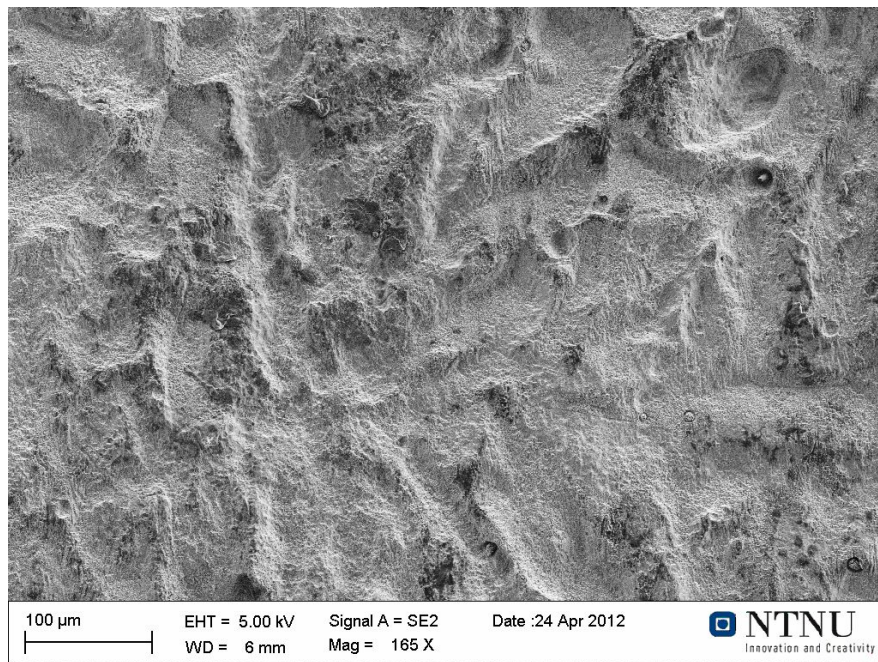
(b) 165 X Magnification

Figure 4.14: SEM pictures of the AlZnIn sample without applied AC voltage

Figure 4.15 shows two microscopic pictures of the sample exposed to 1 V AC. A large corroded area is shown in Figure 4.15 (a). The surface inside this area is rough compared to the surroundings. The area is characterized by a number of hemispherical pits that have merged to form a large corroded area. The picture is taken close to the edge of the sample. Figure 4.15 (b), which is a picture taken in the middle of the sample, shows a small pit on the surface. This pit has a smooth surface and is surrounded by small newly nucleated pits.
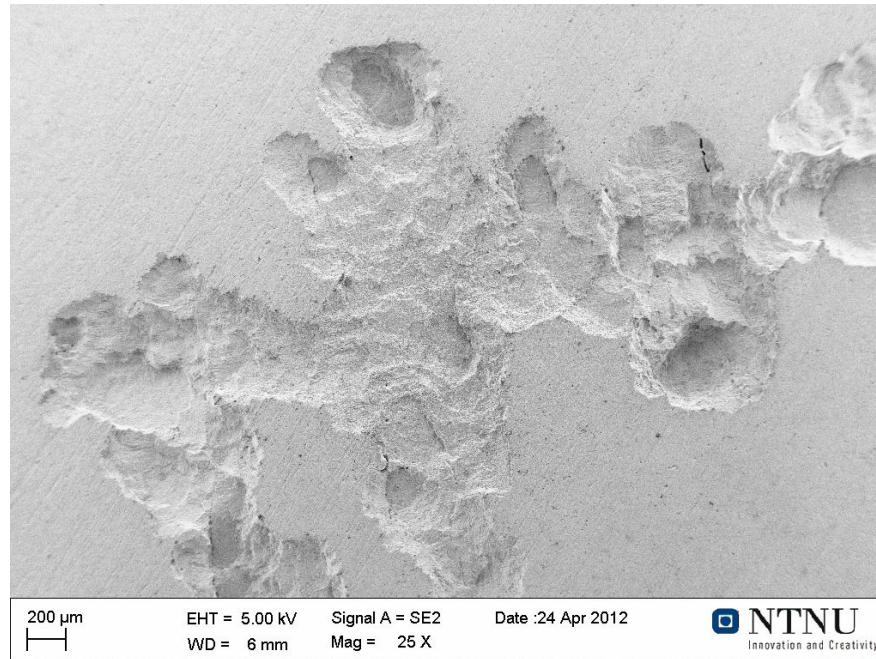
(a) 25 X Magnification
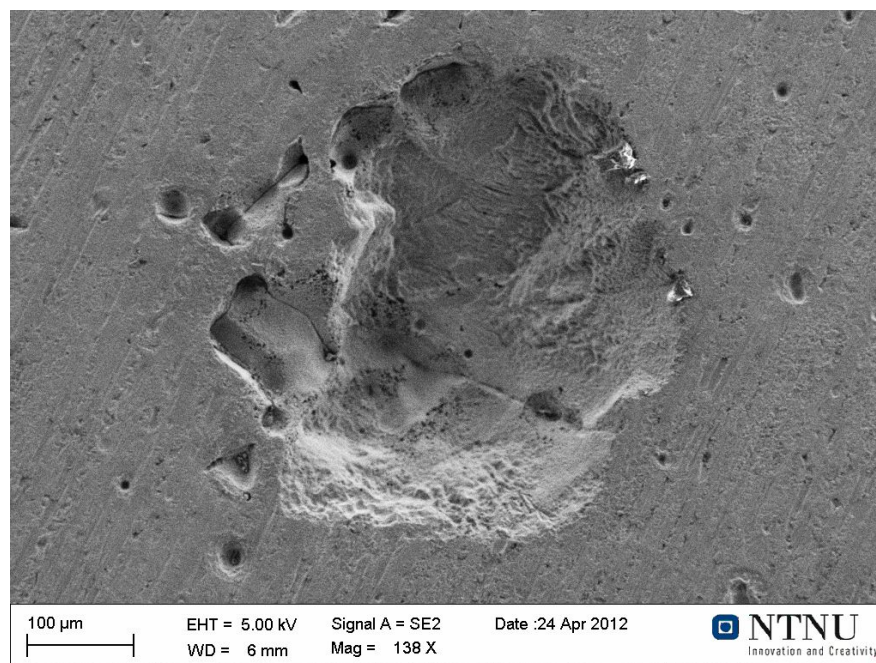
(b) 138 X Magnification

Figure 4.15: SEM pictures of the AlZnIn sample exposed to 1 V AC

A large corroded area can be seen on the sample exposed to 2 V AC (Figure 4.16). The morphology inside the corroded area is very rough compared to the smooth surroundings that can be seen in the bottom right corner. The corroded area is characterized by deep thin holes.

37
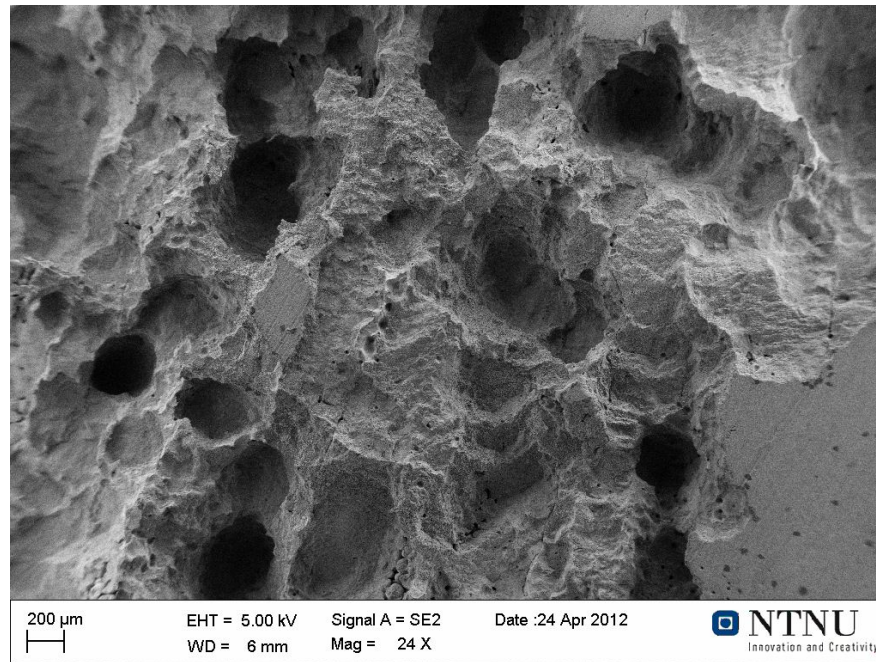
Figure 4.16: SEM picture of the AlZnIn sample exposed to 2 V AC

Three pictures were taken of the sample exposed to 3 V AC (Figure 4.17). Figure 4.17 (a) shows a picture that is taken of the large corroded area on the edge of the sample (Figure 4.6 (d)). This area is characterized by a rough morphology and deep corroded holes. As can be seen from Figure 4.17 (b), the entire surface was covered by small pits. Figure 4.17 (c) shows an enlarged picture of one of these pits. The pit is half spherical and it is characterized by a smooth surface inside.
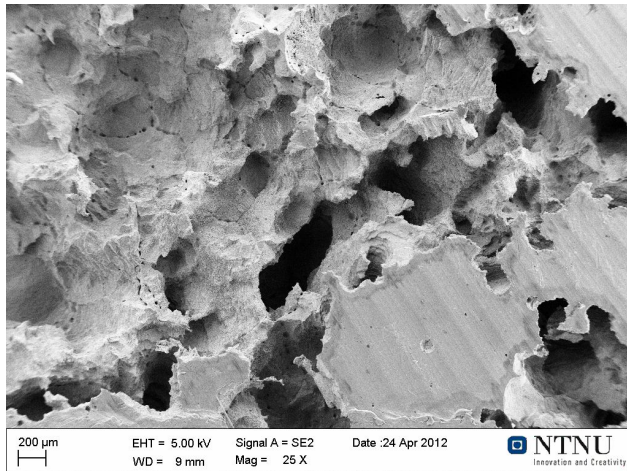
(a) 25 X Magnification
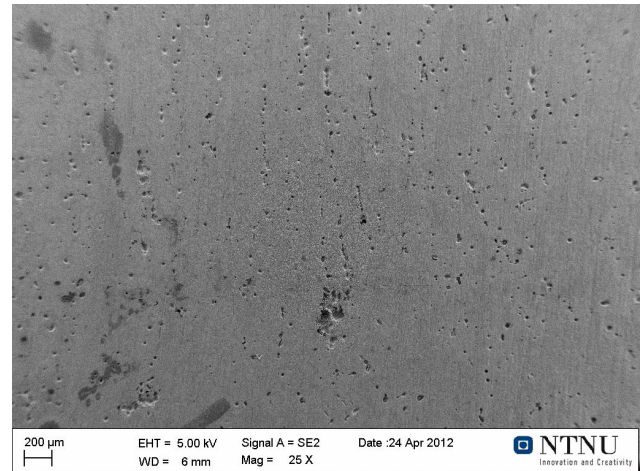
(b) 25 X Magnification
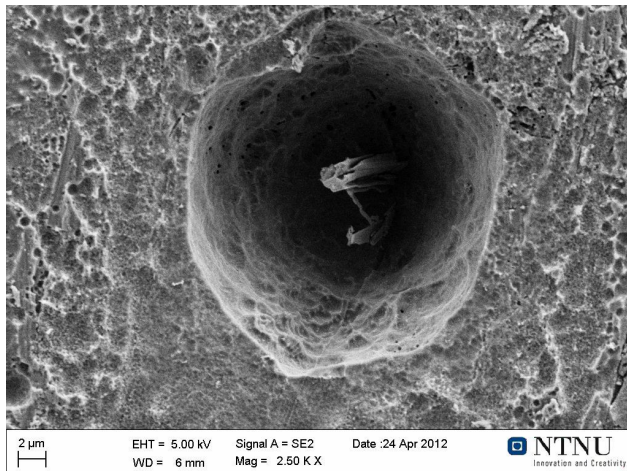
(c) 2500 X Magnification

Figure 4.17: SEM pictures of the AlZnIn sample exposed to 3 V AC

Pictures of the sample exposed to 4 V AC can be seen from Figure 4.18. Figure 4.18 (a) shows that deep pits were formed on the entire surface. One of these pits is shown in Figure 4.18 (b). The pit has sharp edges and a rough surface inside the pit. The grinding strips from the sample preparation can be seen on the surface outside the pit.
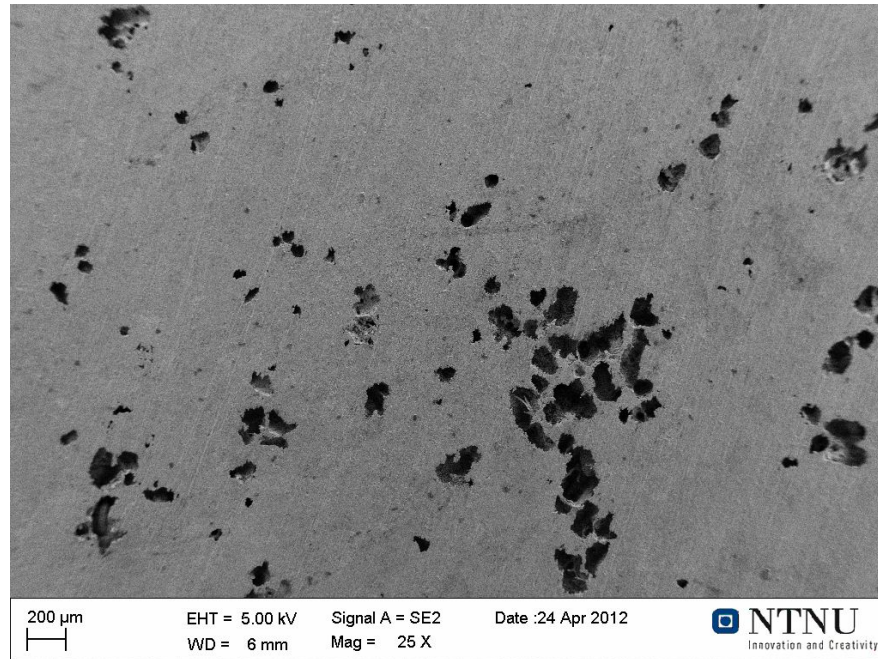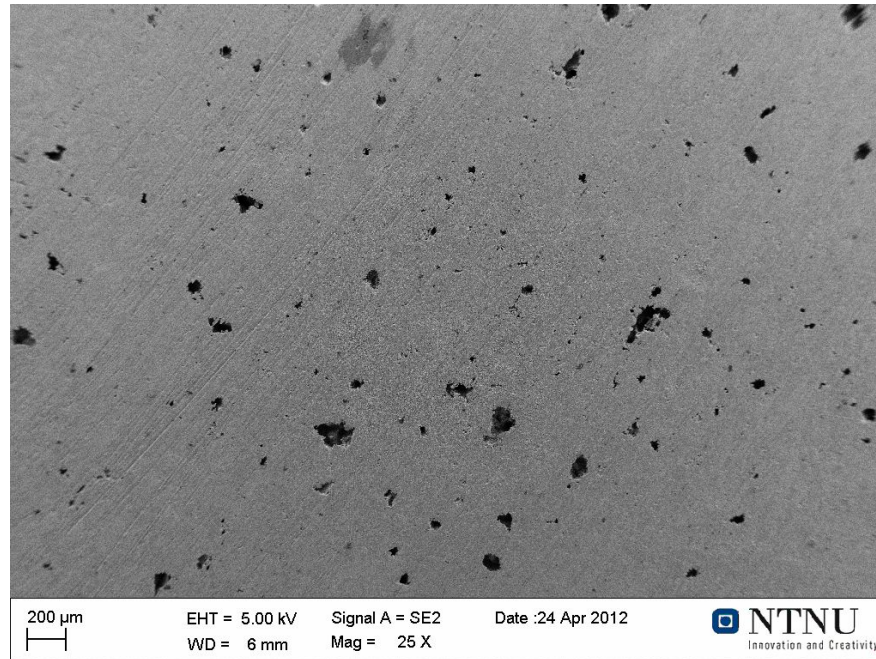
(a) 25 X Magnification
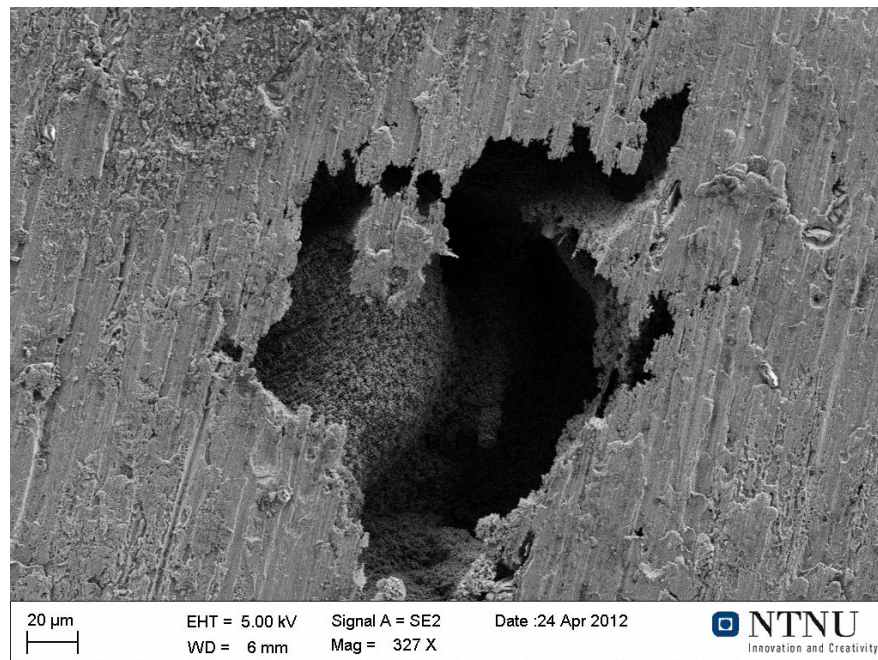
(b) 327 X Magnification

Figure 4.18: SEM pictures of the AlZnIn sample exposed to 4 V AC

The last sample is shown in Figure 4.19. Also in this case, the entire surface was covered by small pits (Figure 4.19 (a)). As can be seen from Figure 4.19 (b), the pits were deep and had a smooth surface. Also for this sample, the grinding strips from the sample preparation is still intact.

(a) 25 X Magnification
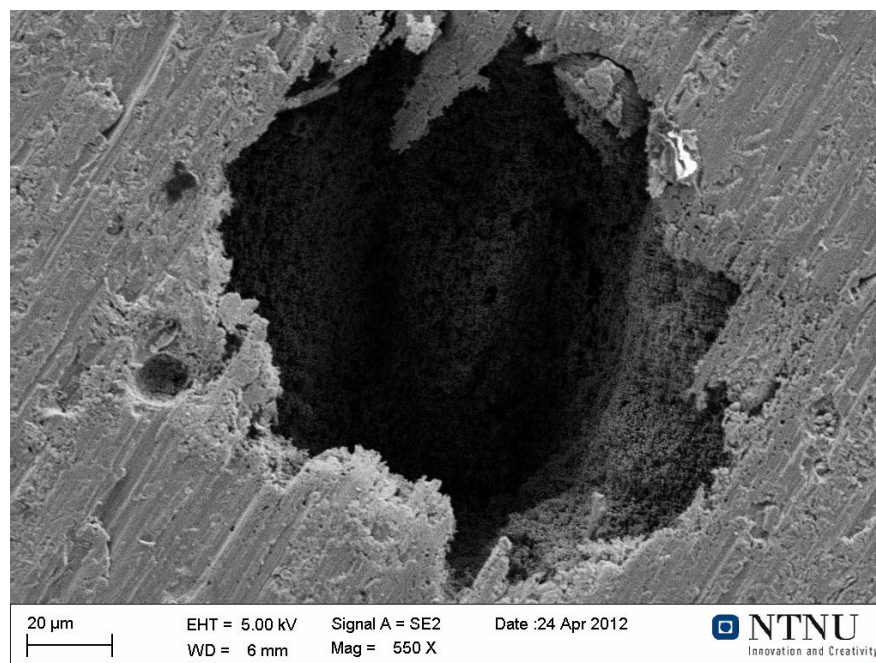
(b) 550 X Magnification

Figure 4.19: SEM pictures of the AlZnIn samples exposed to 5 V AC

Microscopic picture of the steel sample exposed to 3 V AC can be seen in Figure 4.20. The picture shows a smooth surface and this was also the case for all the other steel samples. No pits could be seen on any of the samples.
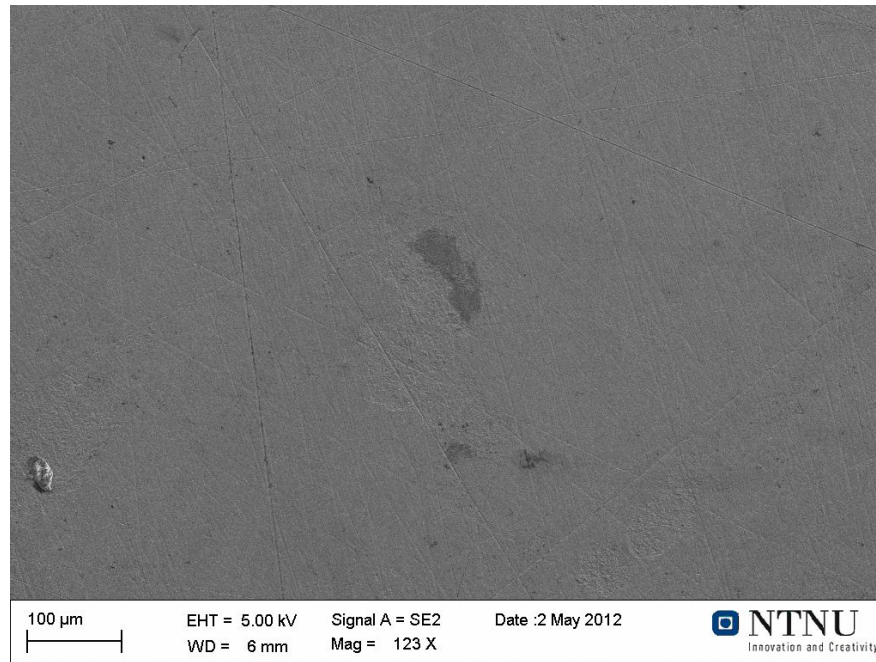
Figure 4.20: SEM picture of the steel sample exposed to 3 V AC

4.4   Polarization curves

Figure 4.21 shows the polarization curves for the AlZnIn samples.
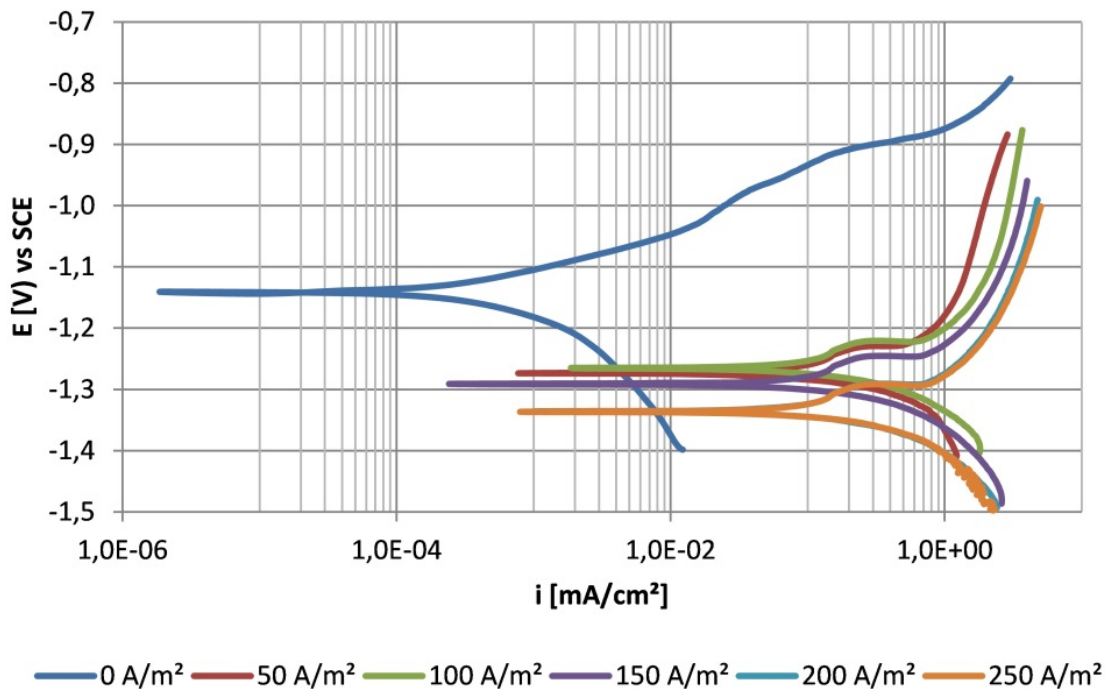
Figure 4.21: Polarization curves for AlZnIn with different values of AC current density

A significant increase in corrosion current density and a decrease in corrosion potential can be seen at the curves without AC compared to those with AC. Within the samples exposed to AC, there are little difference in corrosion current density and corrosion potential. The corrosion current density for the sample without AC is about $10^{-3}mA/cm^2$ and the corrosion potential is about -1,15 V. For the samples exposed to AC the corrosion current density is between $10^{-1}mA/cm^2$ and $1mA/cm^2$ and the corrosion potential varies between -1,25 V and -1,35 V.

4.5 AlZnIn potential vs time

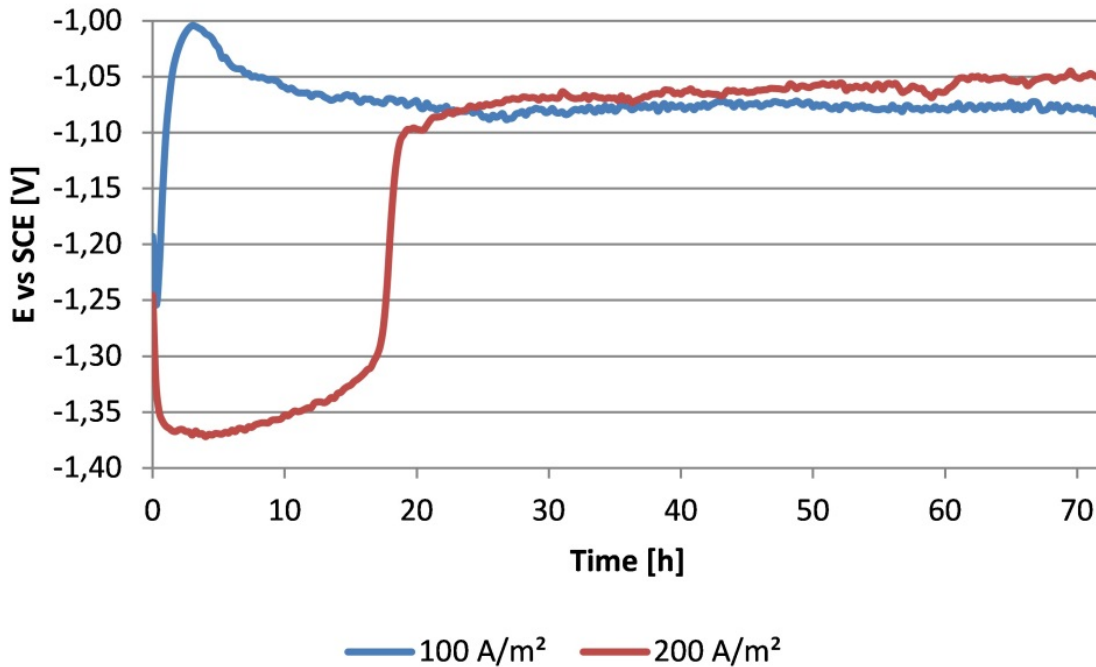The potential vs time curves can be seen from Figure 4.22.

Figure 4.22: Potential vs time for AlZnIn samples with superimposed AC current.

For the sample exposed to 100 A/m^2, the potential increased from -1,25 V to -1,0 V during the first few hours. This was followed by a slightly decrease the next 25 hours to about -1,08 V which lasted for the remaining exposure time. The sample exposed to 200 A/m^2 experienced a rapid decrease from -1,25 V to -1,37 V during the first couple of hours. After this, the potential increased slightly to -1,31 V after 18 hours before a rapid increase to -1,10 V could be seen. For the rest of the exposure time the potential increased slightly to -1,05 V.

Chapter 5

Discussion

5.1 Formation of calcareous deposits

Figure 4.1 shows that calcareous deposits had precipitated on the steel surface after the pre exposure. The morphology of the layer is quite smooth which indicates that the precipitation has occurred uniformly on the entire surface. However, a small crack can be seen in the middle of the surface which could indicate that hydrogen evolution has caused damage of the layer. Because of this crack, a rapid increase in current density should be expected from Figure 4.3. Since no increase is observed, it is possible that the crack has occurred after the experiment when the sample was removed from the setup.

The potential of the steel samples can be seen from Figure 4.2. During the first 300 hours, the potential is quite unstable, varying from approximately -0,8 V to -1,05 V. After 340 hours, the potential increased to about -0,3 V and the reference electrode was changed. The potential was then stabilized at -1,05 V during the remaining exposure time. Since it is electrochemical impossible for carbon steel in galvanic contact with AlZnIn to reach a potential of -0,3 V vs SCE, it is believed that the first reference electrode was not operating well. This can also explain the instability of the potential during the first 340 hours. The fact that the potential stabilized at -1,05 V after the reference electrode was changed, indicates also that the first reference electrode did not work properly.

-1,05 V vs SCE has previously been reported to be the galvanic couple potential between carbon steel and AlZnIn. Because of this, it is believed that the potential was about -1,05 V during the whole exposure period and the samples were fully protected during the pre exposure. The KCl solution inside the reference electrode and the electrolyte outside the electrode was still intact when the potential started to increase. The salt bridge and the connections between the reference electrode and the samples were also checked. Everything seemed to be working well and it is not understood why the potential values increased.

Figure 4.3 shows the current density of the samples during the pre exposure. The current density decreased for all samples. Previous studies have shown that high rate of hydrogen evolution will lead to cracks in the calcareous layer, resulting in a rapid increase in the current density. Such rapid increases could be observed for some of the samples, but in a much smaller extent than previously reported [2]. The current density of sample 2, 3, 4 and 6 decreased with a relative high rate during the first 100 hours. The reason for this is due to formation of $Mg(OH)_2$ and $CaCO_3$. After approximately 100 hours, the entire surface was covered by calcareous deposits and the access to oxygen on the steel surface was reduced. This means that hydrogen evolution became the dominating reduction reaction and this reaction has less impact on the calcareous deposits formation than oxygen reduction. Consequently, the current density became more stable and the curves flattens out after about 100 hours.

Previous reports have stated that the current density vs time curve is characterized by an upper plateau followed by a decrease in current density after approximately 30 - 50 hours [6]. This was not the case in this experiment where the current density showed a clear decrease from the start. Due to this observation, it

seems like the inner $Mg(OH)_2$ layer, which is the first layer to precipitate, has better protective properties than expected. Another explanation could be that $CaCO_3$ precipitates immediately at the surface when the experiment starts.

The initial and final current densities of the samples can be seen from Table 4.1. A significant decrease in current density from start to end can be seen for all samples. Sample 1 and sample 5 distinguishes from the other samples with a relatively low initial current density. Since the conditions were equal for all samples, the theoretical current density should be equal as well for the different samples. However, the current density is dependent on the surface conditions like morphology and chemical environment. It is possible that an oxide layer could have been formed at the surfaces. This can explain the difference in initial current density.

The most important thing due to this work is that the current density stabilizes and that the final current density is almost the same. The protection current from the sacrificial anode is of great importance when it comes to the properties of calcareous deposits. The fact that the final current densities were quite similar for most of the samples, indicates that the calcareous deposits on the samples had almost equal properties. This means that the conditions were almost the same for all samples in the remaining experiments. However, it should be noted that the final current density of sample 3 was a bit lower than the others. The current vs time curve for sample 3 decreases during the whole exposure time and it seems like the hydrogen evolution has not caused any damage of the layer. It is therefore possible that the calcareous deposits at sample 3 had different properties than the others, which might have had an impact for the further experiments.

5.2 Cathodic protection with superimposed AC voltage

5.2.1 Macroscopic analysis

All steel samples were covered by calcareous deposits as can be seen from Figure 4.4. Sample 1 and sample 5 had a quite smooth surface compared to the other samples. This indicates that the deposition rate was uniform on these two samples. Previous studies [2] have shown that calcareous deposits will be lifted of the surface and become porous with high values of AC current. This was not the case in this experiment where the calcareous deposits were still intact at all samples after the experiment. One reason for this can be the geometry of the samples. In previous studies [2], snadder sample holders have been used in the experiment. This will give increased pressure at the interface between the salt layer and the steel surface because of the walls surrounding the exposure area. The calcareous deposits will be located at the bottom of a hole which will result in increased pressure. In this experiment, the sample surfaces were plane and the pressure generated from the hydrogen evolution could be released without destroying the calcareous deposits.

Due to the relatively low DC current density of sample 5 and 6 (Fig. 4.10), it is believed that the calcareous deposits gave a high protection to these samples. This effect can not be seen at the pictures in Figure 4.4 where the calcareous layer looks similar for all samples. On the other hand, it is difficult to determine the protective properties based on observation of the calcareous layer with the naked eye. To get a better insight to the protective properties of the calcareous layer, EDS analysis could be done to determine the chemical composition. This was not done in this experiment since all corrosion products had to be removed due to the weight loss measurements. The best way to look at the protection of the steel samples in this work is by analyzing the DC current which shows a clear reduction for the samples exposed to 4 and 5 V AC.

The macroscopic pictures from Figure 4.6 shows that pitting becomes the dominating corrosion mechanism when the AC current increases. Large cathodic amplitudes will produce an alkaline environment on the AlZnIn surface. This might prevent the formation of $ZnAl_2O_4$ and favour the formation of $Al(OH)_3$. In this way the AlZnIn surface becomes passive which can explain why pitting appears on the entire surface at high AC current densities. The reason why the large corroded areas occur might be due to segregation of In rich zones. During casting of AlZnIn sacrificial anodes the molten phase will have higher solubility than the solid phase. The In particles will follow the solidification boundary which will cause an uneven distribution of In zones in the material. Since the active dissolution occurs at the In rich zones, this can explain the corroded areas.

The samples exposed to 4 and 5 V AC have a more uniform distribution and deeper pits than the other samples. A possible reason for this could be a passive film, the large amount of corrosion products and hydrogen gas occurring at the AlZnIn surface (Figure 4.5). This means that the nucleated pits will not expand but they will grow deeper only in the areas with high In concentrations. The absence of large corroded areas and consequently small anodic areas can also explain the relatively low DC current at these samples.

It is obvious from Figure 4.5 that a white layer was formed at the AlZnIn samples and the amount of this layer increased with increasing AC voltage. This could be either corrosion products, calcareous deposits or a combination of these. From Figure 4.5 (a) - (d) it is clear that this layer is present in the corroded areas and it is dragged in the direction of the hydrogen bubbles. This indicates that it is corrosion products covering parts of the samples. At the samples exposed to 4 and 5 V AC, this layer covers the entire surface which indicates that the high AC current density has caused high corrosion.

5.2.2 CP parameters

Figure 4.7 shows that all samples had a potential lower than the protection potential of -850 mV vs SCE which indicates that all samples were fully protected. The potential without AC was relatively constant during the exposure time at -1,12 V vs SCE. Once AC was present in the system, the potential dropped to a value between -1,17 V and -1,18 V vs SCE. A clear correlation between AC voltage and DC potential can be seen when AC is present. The potential increases with increasing AC voltage which coincides with what has been reported previously [14]. The difference in potential is relatively large between sample 4 and sample 5 compared to the other samples. This gap between sample 4 and sample 5 compared to the others, can also be seen in AC current density from Figure 4.10.

Sample 4, 5 and 6 are all experience a rapid increase in potential during the early stage of the experiment. This is probably due to stabilization, despite the fact that all samples were exposed to the electrolyte and AC voltage for 30 minutes before the experiment started and the conditions should be equal for all samples. Although there exists literature that states that the galvanic potential will increase with increasing AC current, no explanation exists for this phenomena.

A correlation can be seen between the potential of the samples in Figure 4.7 and the surface morphology of the AlZnIn samples in Figure 4.6. The more the potential increases, the smaller becomes the corroded areas. This can be explained by anodic and cathodic controlled corrosion. When the AC current density increases, the cathodic area will become larger relative to the anodic area, resulting in increased potential towards more anodic values to maintain equilibrium. Another explanation could be that corrosion of steel is the controlling factor of the galvanic potential. The polarization curves of AlZnIn shown in Figure 4.21 shows that the potential is relatively constant with increasing AC, but still below the potential without AC. To get a better understanding of the galvanic potential between steel and AlZnIn with AC involved, polarization curves of both steel and AlZnIn need to be analyzed with different values of AC.

Previous studies [2] have shown that it might be difficult to keep the AC current constant during the experiment. This was also a problem in this work, especially for high current densities as can be seen from Figure 4.8. As expected, the AC current density increases with increasing AC voltage. It has previously been reported that above an AC current density of 20 A/m^2 corrosion might occur [14, 15]. This means that corrosion could potentially happen for all samples in this experiment. It should also be noted that samples 3-6 all have a current density higher than 100 A/m^2 which has been reported as the threshold value for whether you can expect corrosion or not. Corrosion was therefor expected on 4 of the samples. However, Table 4.2 shows that there were not high corrosion rates and Figure 4.20 shows that no pitting corrosion could be seen on the steel samples.

A large gap in AC current density can be seen between the samples exposed to 3 and 4 V AC which indicates that the resistance increases. This is probably due to blocking of the AlZnIn surface. The corrosion products formed on the surface in combination with high rate of hydrogen evolution might affect the corrosion kinetics at the surface. The irregular difference in behavior between the samples exposed to 3 and 4 V AC can be seen at DC current, DC potential, surface morphology and corrosion rate as well as AC current. Intensive

hydrogen evolution at the sacrificial anode was also observed during the whole experiments with the samples exposed to 4 and 5 V AC. It seems like AC current densities higher than 36 A/m^2 for AlZnIn will give cathodic amplitudes high enough to produce a layer of hydrogen gas on the surface. This layer will increase the resistance in the circuit which results in pitting corrosion, increase in DC potential, lowering of the DC protection current density and lowering of corrosion rate.

From Figure 4.10 it can be seen that the DC current density acted differently for each sample. The DC current density of sample 1 without AC was relatively constant during the whole experiment. This was also expected since the conditions were the same as in the pre exposure and calcareous deposits had already been precipitated at the surface. The final current density of sample 1 in the pre exposure was about 0,6 A/m^2 which is consistent with the value of 0,6 - 0,7 A/m^2 during the CP experiment without AC.

When AC is introduced to the system, the initial DC current density increases for all samples. The higher the AC voltage is, the higher is the initial DC current density. This is probably because of increased rate of oxygen reduction. When AC is superimposed to DC current, the steel sample will require more current from the sacrificial anode during the anodic half wave. Consequently, the rate of calcareous deposit precipitation will increase due to the high pH increase. This is also probably the reason why sample 4-6 shows a rapid decrease in DC current density the first couple of hours. The high rate of precipitation of CaCO$_3$ and Mg(OH)$_2$ reduces the access to oxygen at the steel surface which results in decreased current requirement.

All samples except sample 1 experienced a decrease in DC current density during the exposure time. Apart from sample 3 that showed a relatively small reduction in DC current, the difference in DC current density from start to end increases with increasing AC voltage. This is also probably a result of the increasing rate of calcareous deposits precipitation and the following current reduction. The fact that sample 5 and sample 6 have such low values of final DC current density compared to sample 3 and sample 4 shows the large impact of the calcareous deposits on DC current requirement. Another explanation for the low DC current density for these two samples could be passivation and reduced efficiency of the sacrificial anode. The pitting morphology at the AlZnIn samples and increased corrosion rate of steel sample 6 can indicate that.

It was expected that the DC current density should increase with increasing AC voltage due to the large anodic half wave and this was also the case for the initial values. Based on these results, it looks like 3 V AC which gives an AC current density between 300 A/m^2 and 500 A/m^2 for carbon steel, is the most critical values when it comes to DC current requirement from the sacrificial anodes.

5.2.3 Corrosion rates

Sample 1 was under cathodic protection without AC but weight loss measurement gave a corrosion rate of 0,073 mm/year on the steel sample (Table 4.2). It should be noted that the entire steel surface was not coated as described in section 3.2.1 and Figure 3.1 (a). Corrosion was observed for all the samples at the area that was not coated. This area was not exposed to the electrolyte and was therefore not under cathodic protection. However, the area with bare steel was located just above the water level which gave a corrosive environment. Since corrosion was observed at this area for all samples and no pits could be seen on the exposure area for any of the samples in SEM, it is likely that this weight loss was a result of corrosion above the water level and had nothing to do with CP and AC.

The fact that the corrosion rates of sample 1-5 were almost the same, varying between 0,056 and 0,073 mm/year, will also support this theory. No clear difference in corrosion rate as a function of applied AC voltage could be seen for the steel samples. This indicates that the area exposed to the electrolyte was fully protected and no corrosion occurred in this area. However, the sample exposed to 5 V AC had a corrosion rate of 0,097 mm/year and differed from the other samples. No corrosion could be seen at the exposure area of this sample, neither with the naked eye or in SEM.

One explanation for the high corrosion rate could be that the high rate of hydrogen evolution could cause the coating to be lifted from the surface. Cathodic disbonding is a well known problem that occurs on cathodically protected steel and this problem is more likely to occur with increasing hydrogen evolution and pH. However, the entire surface was investigated and no pits could be seen. It is therefore likely that the weight loss is due to uniform corrosion and not pitting corrosion that has been reported as the characteristic

corrosion mechanism for AC corrosion. It is also possible that the weight loss of the last steel sample is a result of sources of errors in the measurements. 0,097 mm/year is a quite low corrosion rate and it is likely to think that all steel samples were protected.

Due to protection current from sacrificial anode, it is difficult to explain why the corrosion rate of the steel sample exposed to 4 V AC is almost the same as the other samples with lower value of AC. The corrosion rate due to protection current for the sacrificial anode exposed to 4 V AC is less than half of the sample exposed to 3 V AC. Previous studies have shown that the corrosion rate of steel under cathodic protection will increase with increasing AC current. It was therefore expected that either the steel corrosion rate or protection current should increase with increasing AC voltage. The surface morphology of the sacrificial anodes shows that pitting corrosion becomes dominating with increased AC voltage resulting in reduction in anode efficiency. This can explain the reduction in DC current density and the high corrosion rate of steel sample 6, but not the low corrosion rate of steel sample 5.

As expected, the corrosion rates were higher for the AlZnIn samples than for the steel samples. Within the AlZnIn samples, no clear correlation could be seen between applied AC current and corrosion rate. There was a large gap between the corrosion rates of the samples with and without AC. Sample 2 has more than twice the corrosion rate of sample 1. This is also supported by the polarization curves in Figure 4.21. The sample without AC stands out from the other samples both in corrosion potential and corrosion current density. This indicates that the current requirement for the steel samples might not be the only reason why the AlZnIn samples with AC have higher corrosion rates than those without AC. Self corrosion of the AlZnIn samples might also give a significant contribution to the corrosion rate when AC is present as can be seen from Table 4.3 and Figure 4.13.

There have previously been reported that the amount of AC corrosion on cathodically protected steel depends on the AC current density and that the probability of AC corrosion increases with increasing AC current density [14, 15]. Because of this, it was surprising that the corrosion rates of the AlZnIn samples exposed to 4 and 5 V AC were lower than the samples exposed to 1, 2 and 3 V AC. This is also reflected by Figure 4.10 which shows that sample 5 and sample 6 have lower DC current density than the other samples exposed to AC. Sample 5 has actually lower final current density than the sample without AC. As previously discussed, this could be due to high hydrogen evolution on the sacrificial anode. Another explanation could be that the high AC current density will increase the reduction reaction rate on the steel surface. This will lead to higher rate of precipitation of $CaCO_3$ and $Mg(OH)_2$ and consequently a more protective layer on the surface. From Figure 4.4 it can be seen that the calcareous deposits on sample 5 and 6 were still intact and covered the entire surface. However, it is not possible to estimate the protection properties of the calcareous deposits based on these macroscopic pictures since all samples are fully covered.

No correlation between the self corrosion rates of the AlZnIn samples from Table 4.3 can be seen. The self corrosion rates of sample 2, 4 and 5 are almost the same, varying from 0,15 to 0,17 mm/year. The other samples have lower self corrosion rates and the sample without AC has actually no self corrosion. The correlation between self corrosion rate and AC current density is not understood and can not be explained. It is believed that AC has an impact on the self corrosion due to the fact that the sample without AC has no self corrosion. However, within the samples exposed to AC, neither the macroscopic and microscopic study of the surfaces, the AC current density or the DC potential can explain why sample 3 and 6 have lower self corrosion rates than the others.

The corrosion rate due to protection of the steel samples shows a more clear correlation between corrosion rate and AC current density, especially for the 4 samples with lowest AC current density. The corrosion rate increases with increasing AC current density for these samples which is probably due to the high anodic amplitudes and consequently increased current requirement for the steel samples. As previously mentioned, the drop in protection corrosion rates for the two last samples can be a result of increased precipitation of calcareous deposits or passivation of the sacrificial anodes, but this theory does not explain why sample 6 has higher protection corrosion rate than sample 5.

The correlation between the corrosion rates of AlZnIn and applied AC current in this work is not entirely understood. One possibility might be that there are source of error in the measurements. The total corrosion rates are based on weight loss measurements. Each AlZnIn sample was cleaned, weighted, painted and stored for 12 hours before the experiment started. They were cleaned and weighted immediately after the

experiment. There might have been impurities at the samples which have affected the weight loss values both before and after the experiment. On the other hand, such impurities should not make big difference since the samples were cleaned and the possible impurities are in a micro scale. It should also be noted that the AC current density for the samples exposed to 4 and 5 V AC was very high. Such high AC current densities might have caused noise in the logging equipment which have affected the measurements. Parallel experiment should have been done to correct for sources of error. Since there are only one measurement per AC voltage, there exists some uncertainties in the experiments.

5.3 SEM characterization

All the AlZnIn samples showed a rough surface in the corroded areas. The depth of the pits increased with increasing AC current. For pure Al, this is explained by the increased amount of Al concentration inside the pits and the following pH increase [21]. However, because of the hydrogen evolution during the cathodic half wave, AlZnIn might become passive when AC is present. This can be explained by the increased pH at the surface during the cathodic cycle which might force Reaction (2.16) to the right and produce more $Al(OH)_3$ in addition of precipitated calcareous deposits. In this way the Al matrix might be repassivated even in the presence of Indium. A white layer could also be seen on all the AlZnIn samples during and after the experiment (Figure 4.5). The amount of this layer was higher in the corroded areas, which indicates that corrosion products and calcareous deposits precipitated at the surface.

It has previously been reported that the surface morphology of corroded AlZnIn is characterized by spherical pits with a relatively smooth surface [19]. This is recognizable from the SEM pictures of the samples exposed to 1, 2 and 3 V AC. The sample without any AC has corroded areas with a rough surface while the two samples exposed to 4 and 5 V AC have deep pits with sharp edges. This indicates that the AC current has an impact of the pitting morphology. As previously mentioned, high AC current results in high amount of dissolved Al inside the pit pores. Consequently the environment inside the pits becomes highly corrosive which will result in hollowing of the pits. This might be the reason why the pits on the samples exposed to 4 and 5 V AC are deep and have sharp edges.

The sample with highest pitting population density seems to be the sample exposed to 3 V AC (Figure 4.17 (b)). This is not consistent with previous reports about Al that claims that the population density decreases with increasing AC current density. However, it should be noted that the existing theory on this subject is based on pure Aluminum. No published work on the effect of AC on AlZnIn was found. One possible reason for the large areas without corrosion at the samples exposed to 0, 1 and 2 V AC could be that Zn plays a significant role at low AC current densities. The amplitudes during the cathodic cycles are not large enough to obtain the alkaline environment required to produce $Al(OH)_3$. This means that the pH value will be kept at a relatively low value and the formation of $ZnAlO_4$ will be the dominating reaction at the surface. Uniform corrosion will then be the dominating corrosion mechanism and this can explain the smooth surface around the corroded areas at the samples with low AC current density.

It should be noted that the grinding strips can be seen at the surface on the samples exposed to 4 and 5 V AC. The strips are much clearer on these samples than the other samples. This may suggest that the grinding strips have corroded at the samples with lower AC voltage and corrosion has occurred at the entire surface. In the case of the samples exposed to 4 and 5 V AC it seems like the corrosion has occurred inside the pits and the rest of the surface has been cathodic. This might have resulted in a low anode/cathode ratio and can explain the increase in potential at these two samples.

No pits could be seen at any of the steel samples. The SEM picture of the steel sample with smooth surface showed in Figure 4.20 was representative for all the samples. This indicates that the steel samples were protected and no pitting corrosion occurred. The fact that there were no clear difference between the corrosion rates of the samples exposed to 0-4 V AC indicates also that no AC corrosion had occurred. This is not consistent with previous reports that says that above an AC current of 100 A/m^2 corrosion is to be expected [14, 15]. However, it has also been reported that at high AC current densities calcareous deposits will lift from the surface and leave bare steel exposed to the surface [9, 2] which was not the case in this experiment. It is therefore conceivable that the calcareous deposits have played a significant role in corrosion protection.

5.4   AlZnIn polarization curves

Figure 4.21 shows that the polarization curve without AC stands out from the curves with superimposed AC. The corrosion potential without AC lies above the other curves, while the current requirement is about 10^2-10^3 times higher when AC is present. The reason why the potential decreases and current density increases is probably a result of the change in chemical composition in the metal/electrolyte interface. The electrical double layer will be affected by the rapid switch between anodic and cathodic half cycles. The surface might also be destroyed and become repassivated due to the corrosion product formed during the anodic cycles and high pH during the cathodic cycles. The anodic half cycles might also lower the overpotential which can result in anodic behavior of the material before the equilibrium potential is reached when it is polarized in anodic direction. All these parameters might have had an impact on the kinetics and corrosion mechanisms of AlZnIn. The low corrosion current of the sample without AC compared to the others can give an explanation why the AlZnIn sample without AC in the CP experiment had no self corrosion.

For the samples exposed to AC the curves increased significant during the anodic polarization which is probably due to IR resistance. The IR drop was so severe that the curves could not be corrected. This indicates that there have been a massive resistance factor on the surface. This could be a combination of hydrogen gas created during the cathodic cycles and also corrosion products like calcareous deposits that block the surface. During both the cathodic and anodic part of the polarization curves, high rate of hydrogen evolution was observed which covered the entire surface.

The high rate of hydrogen evolution caused precipitation of calcareous deposits on the surface. This layer was observed on all samples exposed to AC and gives an explanation for the high IR drop in the electrolyte. Since all samples were polarized in anodic direction the precipitation of calcareous deposits started immediately when the experiment started. The low initial potential in addition to the high cathodic amplitudes caused a high increase in pH at the AlZnIn samples. Because of these high amplitudes, the pH was probably high even in the anodic part of the polarization curves. The bubbles itself could also play a significant role in resistance at the surface. The bubbles generated during the cathodic half wave will cover part of the surface and also take up a volume fraction of the electrolyte.

5.5   AlZnIn potential vs time

The corrosion potential of the two samples that were exposed to 100 and 200 A/m^2 is shown in Figure 4.22. The initial potential of -1,25 V$_{SCE}$ was equal for both samples but the potential acted complete different for the two samples when AC current was introduced. A rapid increase in potential was observed for the sample exposed to 100 A/m^2 while the potential decreased for the sample exposed to 200 A/m^2. However, the potential seems to stabilize between -1,05 to -1,10 V$_{SCE}$ after about 20 hours. No correlation could be seen between the two samples in the way the potential acted. The reference electrode was tested before the experiment and the initial potential was identical for the samples. This, in addition to the fact that the potential stabilizes to almost the same potential for each sample, indicates that the reference electrode was operating well.

There are no previously written work found on the free corrosion potential variation of AlZnIn with alternating current. However, there exist some literature when it comes to carbon steel. Goidanich et al. [22] reported that the potential will decrease rapidly for steel when AC is introduced. This is followed by stabilization at a higher potential than the potential measured without AC. The AlZnIn sample exposed to 200 A/m^2 shows a completely identical behavior to that reported for carbon steel. Since the sample with a lower value of AC current acts in the opposite way, it seems like the potential variation of AlZnIn samples is different than for steel. On the other hand, both carbon steel and AlZnIn have in common that the potential stabilizes at a higher potential when AC is present and the potential increases with increasing AC current density.

Before AC is introduced to the system, there is no surface coverage on the AlZnIn sample and the surface remain active. Once AC is introduced large variation in the potential could be observed. The sample with highest AC current density becomes cathodic controlled while the sample with lowest AC current density becomes anodic controlled. The factor that determine either if it is anodic or cathodic controlled could be

the ratio between the anodic and cathodic areas on the surface. The macroscopic pictures of the sacrificial anodes in the CP with AC experiment (Fig. 4.6) showed that the pit distribution increased with increasing AC current density. Due to the large anodic area, the sample might have became cathodic controlled resulting in decreased potential. The sample exposed to 100 A/m^2 may on the other hand have become anodic control due to large cathodic areas. This can explain the potential increase for this sample. However, it is difficult to explain the behavior with only two samples. More experiment with different value of AC current density have to be done to get a better understanding of the phenomena.

Chapter 6

Conclusion

Steel under cathodic protection was protected against AC corrosion at AC current densities up to 1300 A/m^2. All steel samples in this experiment had corrosion rates lower than 0,1 mm/year. This is also supported by microscopic investigation in SEM where no pits could be seen at the steel samples.

The corrosion rate of AlZnIn sacrificial anodes is largely influenced by the AC current density. Corrosion rate of AlZnIn due to protection of steel increased with increasing AC current density up to 300 - 500 A/m^2. At this value the samples became passive due to the alkaline environment occurring on the surface which decreased the corrosion rate of AlZnIn. No self corrosion of AlZnIn was detected without AC. Within the samples exposed to AC, the self corrosion rate varied but no correlation between corrosion rate and AC current density could be seen.

The galvanic potential of steel and AlZnIn increased with increasing AC current density. The reason for this is not entirely understood but it is believed that the pitting morphology at the AlZnIn surface at high AC current density will force the potential to more anodic values. This is due to the decreased anode/cathode ratio at the surface. No difference in calcareous deposits could be seen at the steel samples. Measurement of DC protection current have shown that DC current increases once AC is applied to the circuit. At high AC current densities, the protection current from the sacrificial anode decreases. It is believed that the reason for this is due to passivation of the sacrificial anode.

Analysis of the AlZnIn surfaces have shown that large corroded areas surrounded by smooth surface are characteristic for AC current densities below 30 - 50 A/m^2. Pitting corrosion at the entire surface occurs at higher current densities. This is most likely because of high hydrogen evolution and increased formation of Al(OH)$_3$ at high AC current densities. Large areas of the surface will be covered and blocked from the electrolyte which prevent the nucleated pits to merge with each other and instead grow deeper. This results in higher resistance and decreased efficiency of the sacrificial anode.

The polarization curves have shown that there is a large resistance in the circuit when AC is present due to covering of the surface by corrosion products and bubbles. The corrosion potential of AlZnIn decreases when AC is present and the corrosion current density increases. Measurements of the corrosion potential of AlZnIn has shown that the corrosion potential stabilizes at a higher potential than the initial potential when AlZnIn is exposed to AC over time. The results present in this report have shown that this surface coverings have had a large impact on the corrosion kinetics of AlZnIn.

Chapter 7

Further work

The effect of alternating current on AlZnIn sacrificial anode is not entirely understood. The protection current and corrosion rate decreases at high AC current densities which should be investigated further. EDS analysis of the calcareous deposits and also the AlZnIn surfaces should be done to look deeper into the composition of the surface coverings and the variation in composition with increasing AC. In this way one can decide if it is the calcareous deposits at the steel samples or passivation of AlZnIn that gives decreased corrosion rate at higher AC voltages.

The results in this work have shown that the steel is protected below a certain value of AC current density. Weight loss measurements should have be done at higher current density to investigate the further development of corrosion rate with higher current densities. This will also give an answer about the galvanic potential development. The galvanic potential increases with increasing AC voltage and it should be interesting to see if this trend will continue and maybe exceeds the protection potential. The effectiveness of the sacrificial anode seems to decrease with increasing AC voltage and it should also be paid attention to this development at higher current densities.

The surface morphology of AlZnIn can also be investigated further. The depths of the pits is not identified properly and this can be done by cutting the samples and study the cross section. This can also give the opportunity to study the variation in composition close to the surface compared to the base material.

The results of the potential variation with time for AlZnIn with applied AC is not sufficient to draw conclusions. Since the potential of only two samples with different AC current density was measured with completely opposite behavior, it is difficult to get a understanding of the mechanisms involved. The potential should have been measured on more samples with different AC current densities to investigate the correlation between potential and AC current.

Bibliography

[1] R. Johnsen, "Cathodic protection," *NTNU*, 2008.

[2] L. Lilleby, "Effect of ac current on calcareous deposits," Master's thesis, NTNU, Trondheim, 2009.

[3] P. Roberge, *Handbook of corrosion engineering*, ser. Products Liability Series, R. Esposito, Ed. New York: McGrow-Hill, 1999.

[4] C. Barchiche, C. Deslouis, D. Festy, O. Gil, P. Refait, S. Touzain, and B. Tribollet, *Characterization of calcareous deposits in artificial seawater by impedance techniques 3-Deposit of CaCO3 in the presence of Mg(II)*, E. Acta, Ed. Science direct, 2003, vol. 48.

[5] A. Neville and A. Morizot, *Calcareous scales formed by cathodic protection - an assessment of characteristics and kinetics*, J. of Crystal growth, Ed. Edinburgh, UK: N.H Elsevier, 2002, vol. 243.

[6] K. Mantel, W. Hartt, and T.-Y. Chen, *Substrate, Surface Finish and Flow Rate Influences on Calcareous Deposit Structure.* CORROSION, 1992, vol. 48, no. 6.

[7] C. Deslouis, A. Doncescu, D. Festy, O. Gil, V. Maillot, S. Touizan, and B. Tribollet, *Kinetics and Characterization of Calcareous Deposits under Cathodic Protection in Natural Seawater*, M. S. Forum, Ed. Switverland: Trans Tech Publications, 1998, vol. 289-292.

[8] T. Okstad, . Rannestad, R. Johnsen, and K. Nisancioglu, "Significance of hydrogen evolution during cathodic protection," *CORROSION 2007*, no. 07079, 2007.

[9] W. Ailor, S. Dean, and F. Haynie, *Corrosion in Natural Environment.* Philadelphia: American Society for Testing and Materials, 1974.

[10] W. Hartt, *Designing Cathodic Protection Systems for Marine Structures and Vehicles*, H. Hack, Ed. ASTM, 1999.

[11] J. Yan, R. White, and R. Griffin, "Parametric studies of the formation of calcareous deposits on cathodically protected steel in seawater," University of South Carolina, Tech. Rep., 1993.

[12] J. Nilsson and S. Riedel, *Electrical circuits.* Pearson Education, 2011.

[13] Z. Panossian, E. Laurino, S. Filho, J. Oliver, N. Almeida, G. Pimenta, M. Filho, J. Albertini, and D. Silva, "Evaluation of ac corrosion pipeline buried using ac-probe," no. 11321. Houston, Texas: NACE International, 2011.

[14] R. Gummow, R. Wakelin, and S. Segall, "Ac corrosion - a new challenge to pipeline integrity," in *CORROSION 98*, no. 566. Houston, Texas: NACE International, 1998, pp. 1–18.

[15] R. Ellis, "Ac induced corrosion on onshore pipelines, a case history." 2001.

[16] M. Yunovich and N. Thompson, "Ac corrosion: Corrosion rate and mitigation requirements," in *CORROSION 2004*, no. 04206. New Orleans: NACE International, 2004.

[17] F. Galsgaard and N. Nielsen, "Ac / dc interference corrosion in pipelines." MetriCorr, 2006.

[18] A. Palmer and R. King, *Subsea Pipeline Engineering*, 2nd ed. Oklahoma: PennWell Corporation, 2008.

[19] A. Munoz, S. Saidman, and J. Bessone, "Corrosion of an alznin alloy in chloride media," *Corrosion science*, vol. 44, pp. 2171 – 2182, 2002.

[20] S. Hejian and H. Shizhong, "Zn's role in dissolution of al sacrificial anodes," *Chin. J. Oceanol. LimNol.*, vol. 8, pp. 354–362, 1990.

[21] M. Tzedaki, I. D. Greave, B. Kernig, J. Hasenclever, and H. Terryn, "Importance of etch film formation during ac controlled pitting of aluminium," Vrije Universiteit Brussel and Hydro Aluminium Bonn, Tech. Rep., 2012.

[22] S. Goidanich, L. Lazzari, and M. Ormellese, "Ac corrosion. part 2: Parameters influencing corrosion rate," *Corrosion science*, vol. 52, pp. 916–922, 2010.

Appendix A

Pre exposure

A.1 Potential

Appendix A1 shows the potential vs time curves for each sample for the pre exposure experiment:
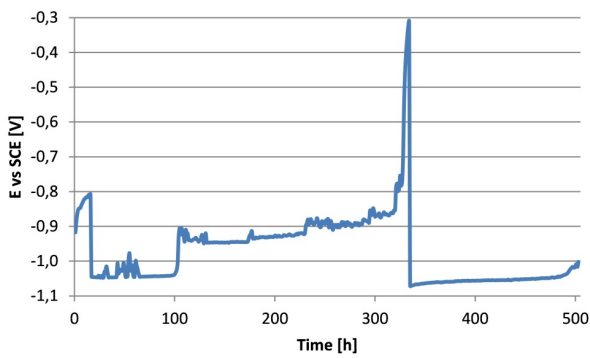
Figure A.1: Sample 1
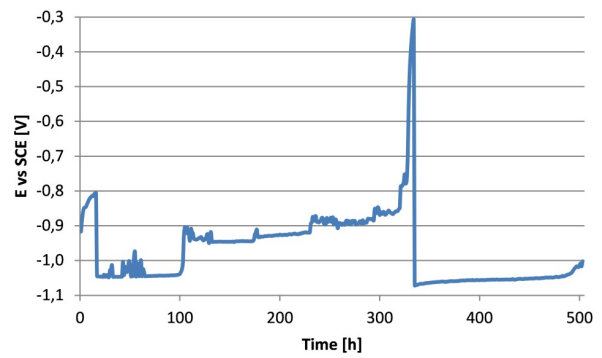
Figure A.2: Sample 2
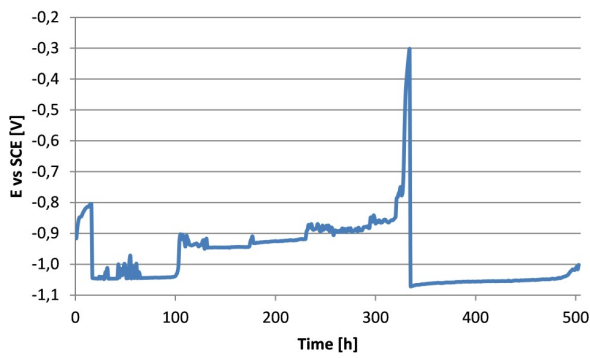
Figure A.3: Sample 3
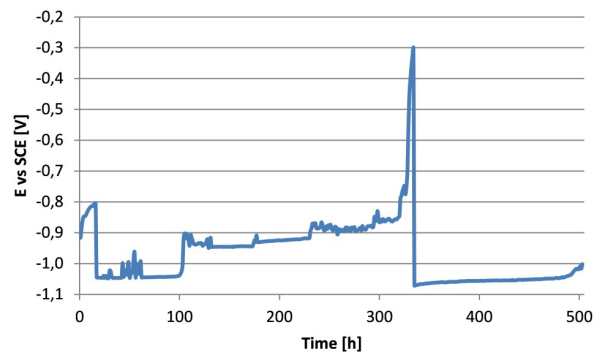
Figure A.4: Sample 4
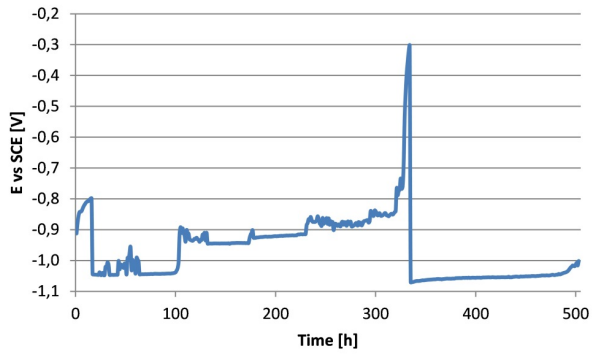
Figure A.5: Sample 5
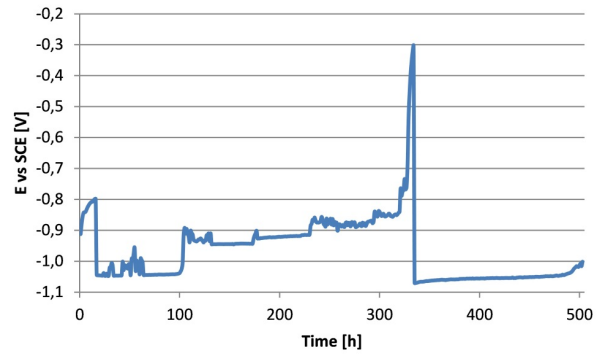
Figure A.6: Sample 6

A.2   DC current density

Appendix A2 shows the DC current density vs time for each sample during the pre exposure:
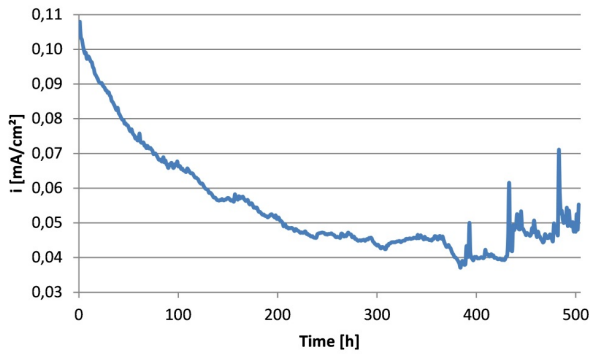
Figure A.7: Sample 1
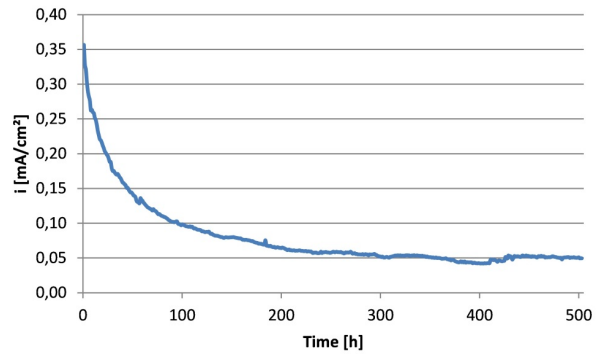
Figure A.8: Sample 2
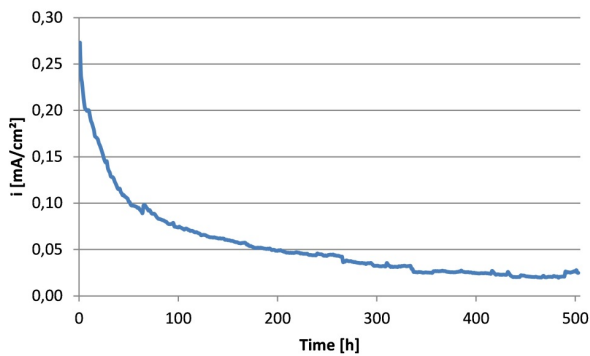
Figure A.9: Sample 3
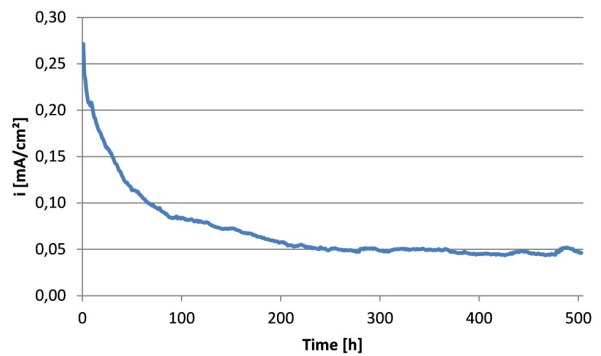
Figure A.10: Sample 4
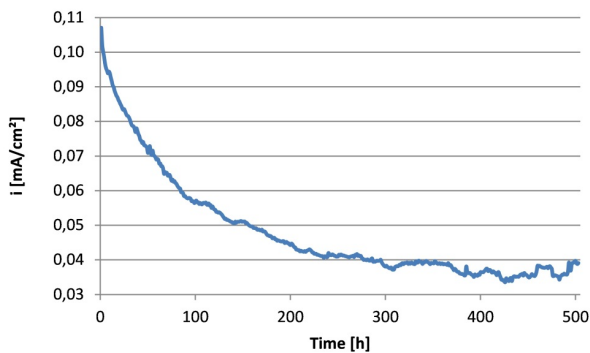
Figure A.11: Sample 5
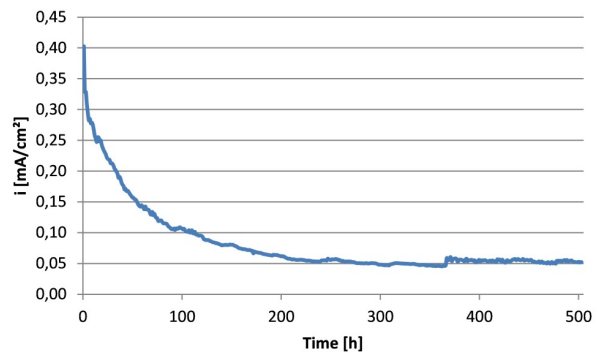
Figure A.12: Sample 6

Appendix B

Cathodic protection with AC

B.1 Potential

Appendix B.1 shows the DC potential for each sample during the CP with AC experiment.
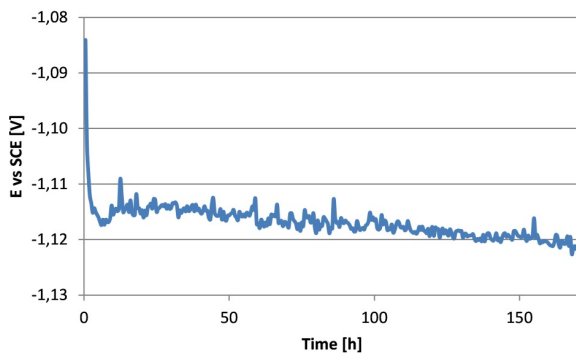
Figure B.1: 0 V AC
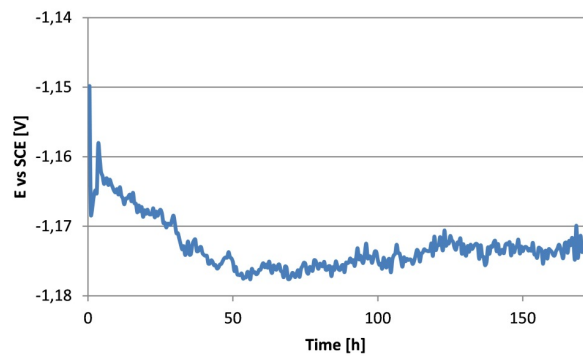
Figure B.2: 1 V AC
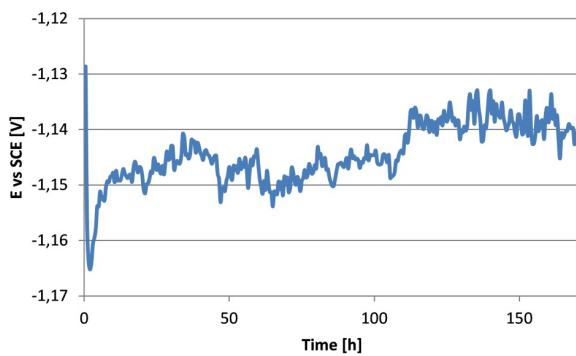
Figure B.3: 2 V AC
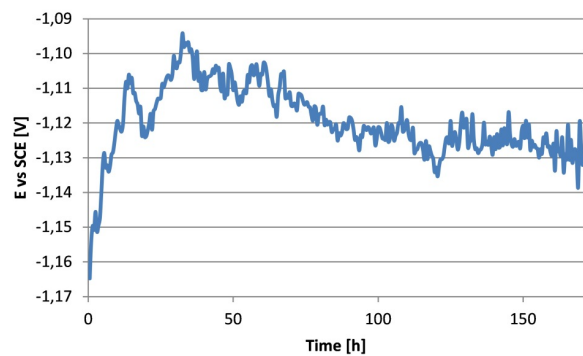
Figure B.4: 3 V AC
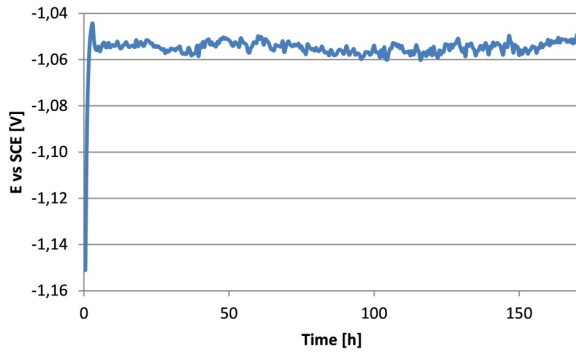
Figure B.5: 4 V AC
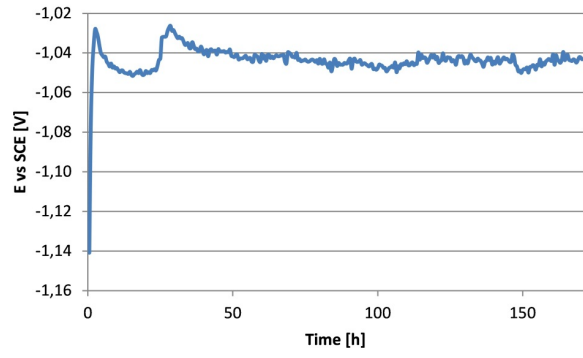
Figure B.6: 5 V AC

B.2   DC current density steel

Appendix B.1 shows the DC current density for each steel sample during the CP with AC experiment.
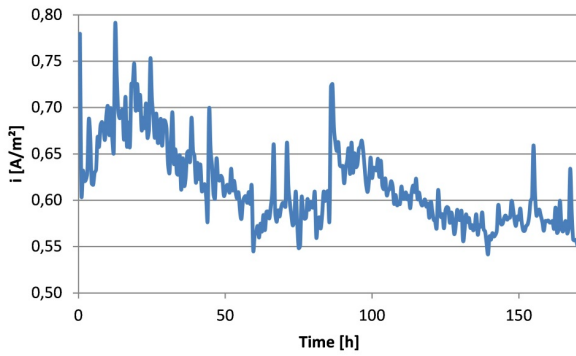
Figure B.7: 0 V AC
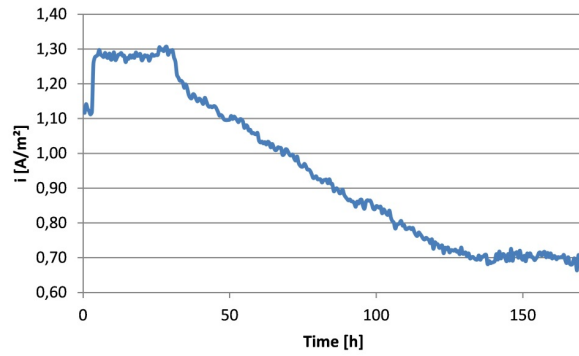
Figure B.8: 1 V AC
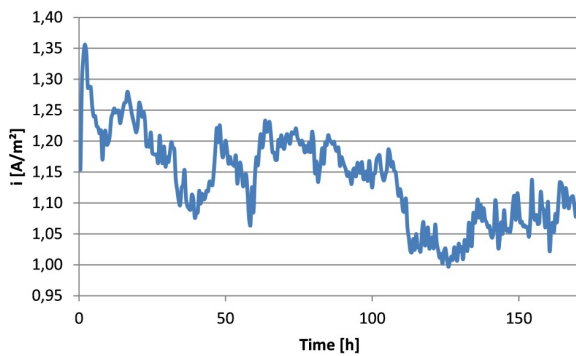
Figure B.9: 2 V AC
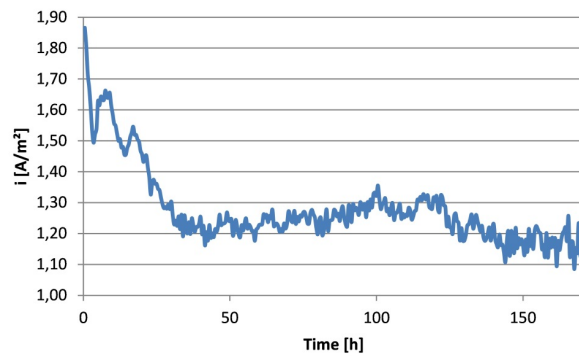
Figure B.10: 3 V AC
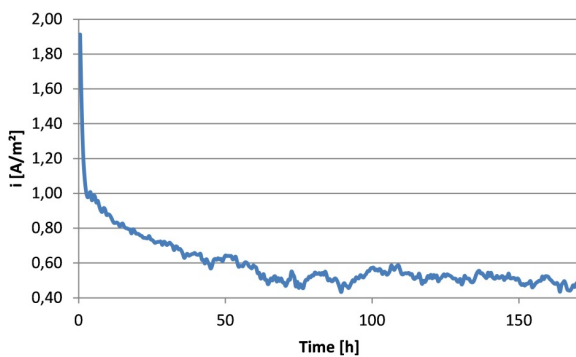
Figure B.11: 4 V AC
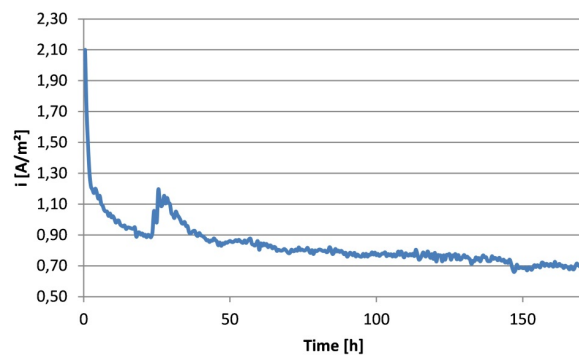
Figure B.12: 5 V AC

B.3 DC current density AlZnIn

Appendix B.3 shows the DC current density for each AlZnIn sample during the CP with AC experiment.
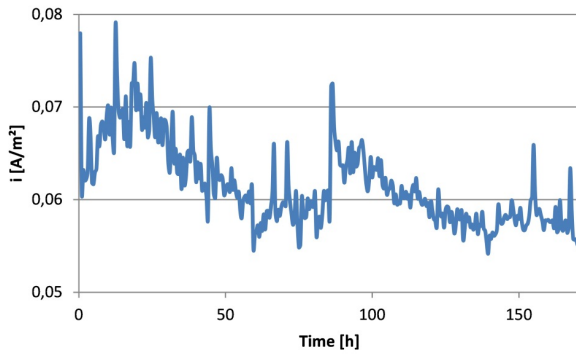
Figure B.13: 0 V AC
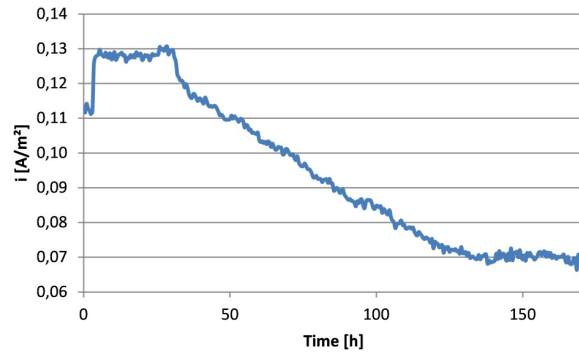
Figure B.14: 1 V AC
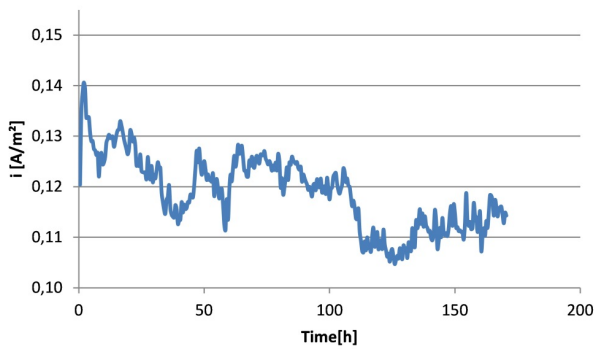
Figure B.15: 2 V AC
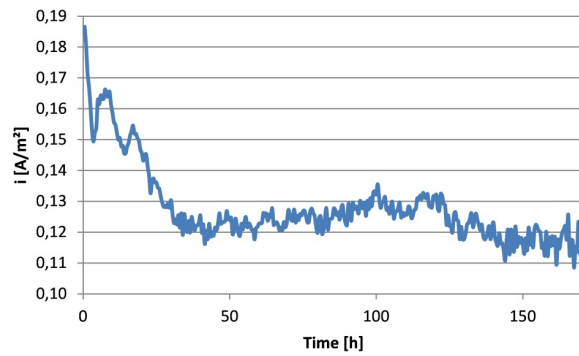
Figure B.16: 3 V AC
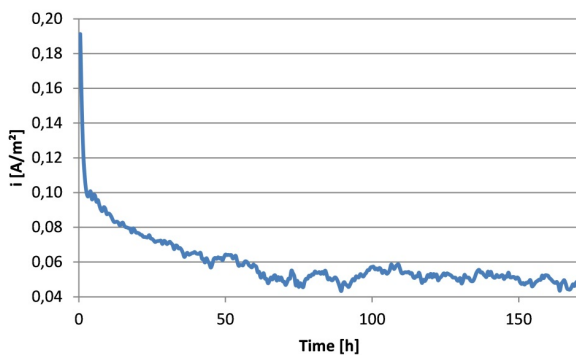
Figure B.17: 4 V AC
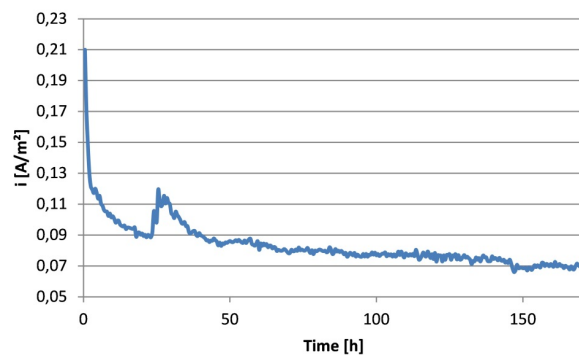
Figure B.18: 5 V AC

B.4   AC current density steel

Appendix B.4 shows the AC current density for each steel sample during the CP with AC experiment.
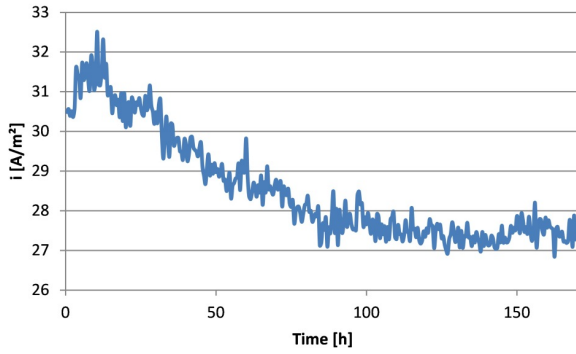
Figure B.19: 1 V AC
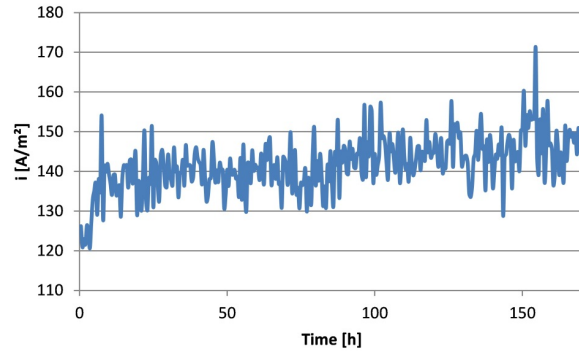
Figure B.20: 2 V AC
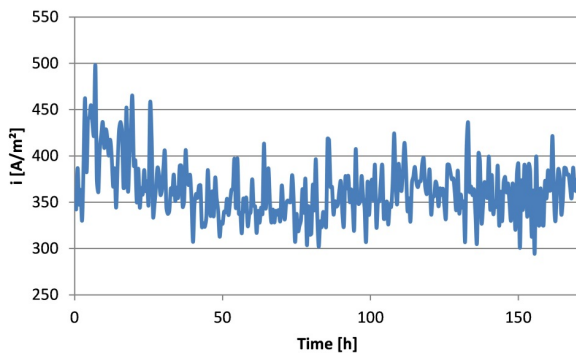
Figure B.21: 3 V AC
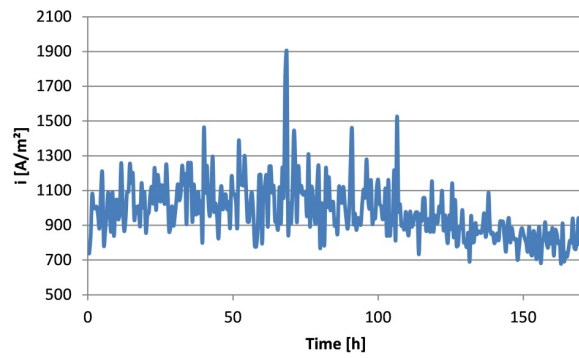
Figure B.22: 4 V AC
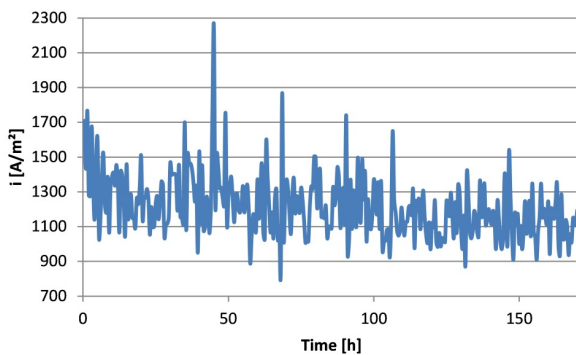
Figure B.23: 5 V AC

B.5   AC current density AlZnIn

Appendix B.5 shows the AC current density for each AlZnIn sample during the CP with AC experiment
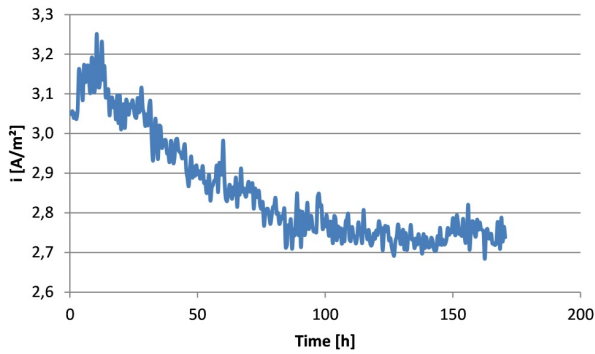
Figure B.24: 1 V AC
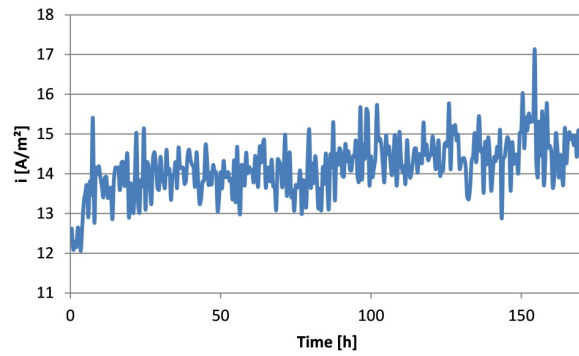
Figure B.25: 2 V AC
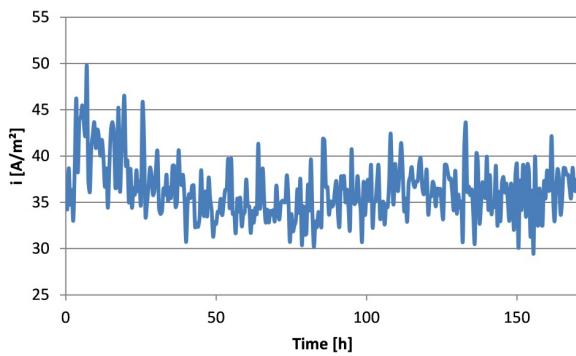
Figure B.26: 3 V AC
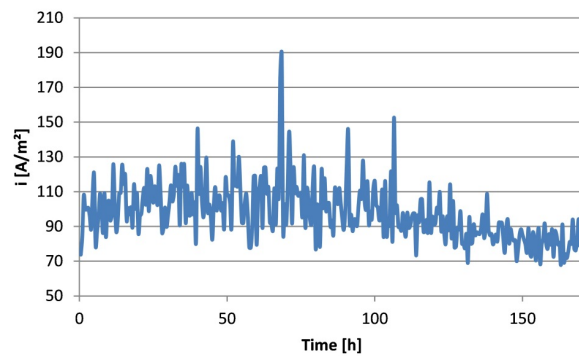
Figure B.27: 4 V AC
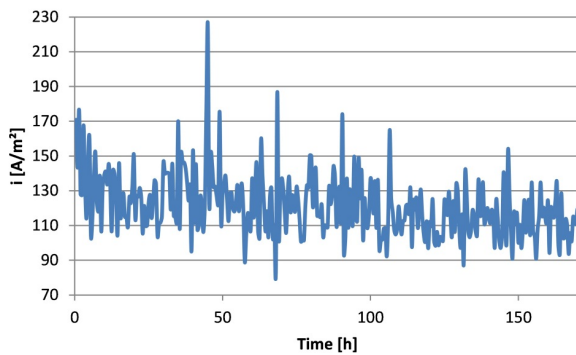
Figure B.28: 5 V AC

Appendix C

AlZnIn polarization curves

Appendix C shows the polarization curve for each AlZnIn sample.
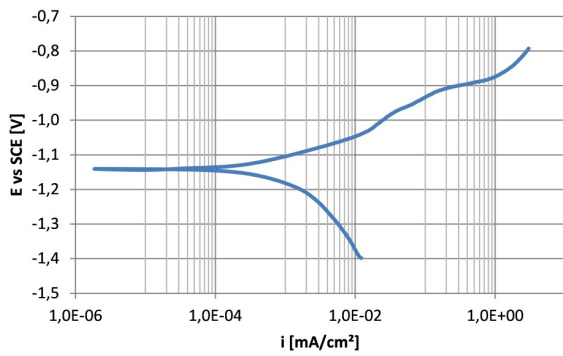
Figure C.1: 0 AC
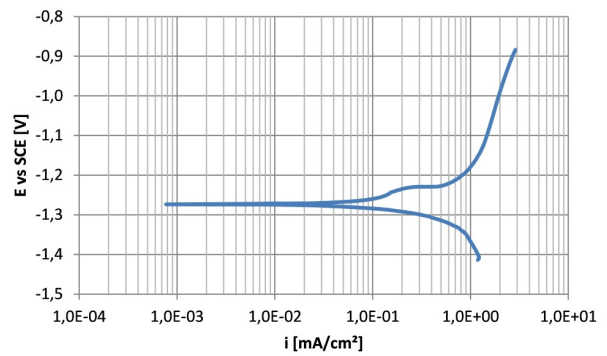
Figure C.2: 50 A/m^2 AC
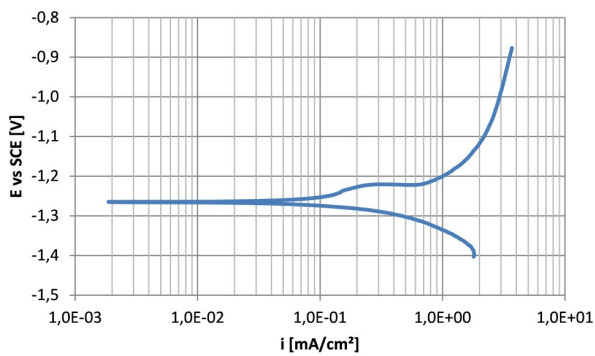
Figure C.3: 100 A/m^{2}AC
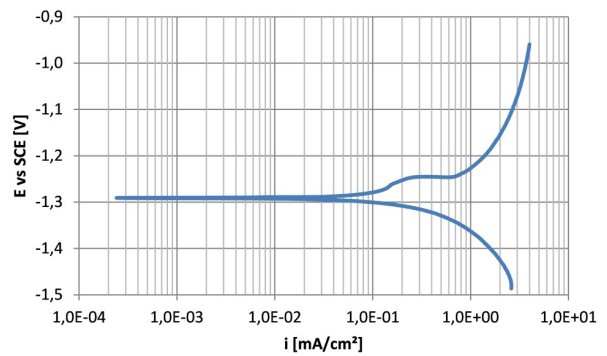
Figure C.4: 150 A/m^2 AC
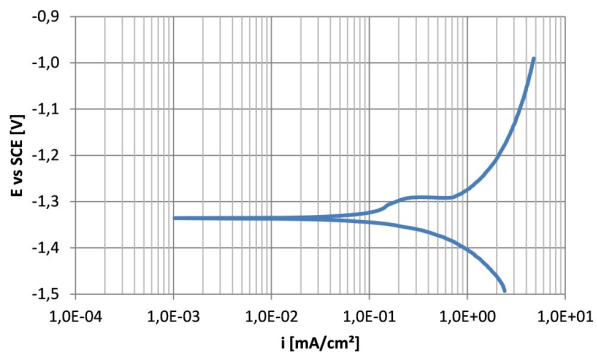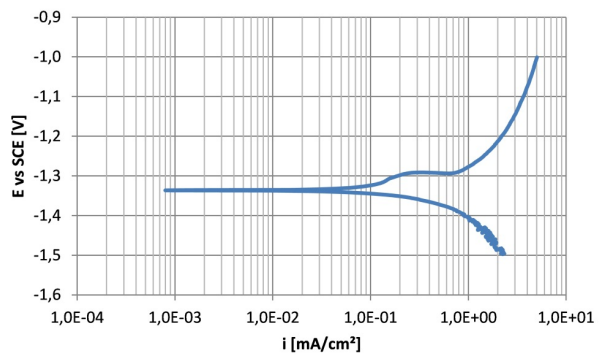
Figure C.5: 200 A/m² AC

Figure C.6: 250 A/m² AC

Appendix D

AlZnIn potential vs time

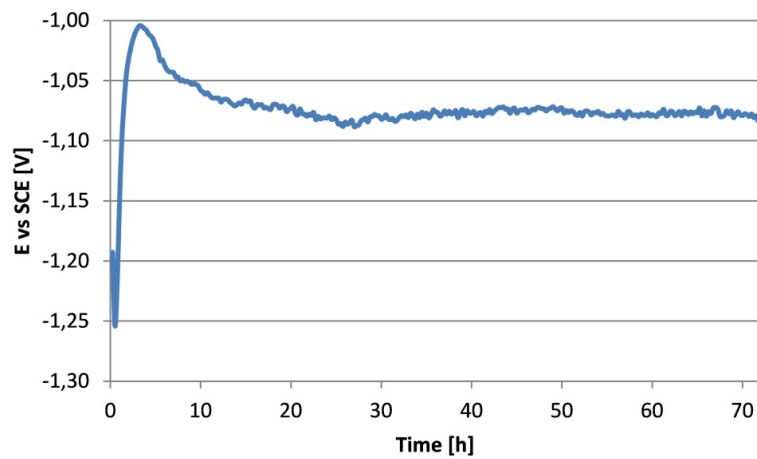Appendix D shows the potential variation with time for each AlZnIn sample.
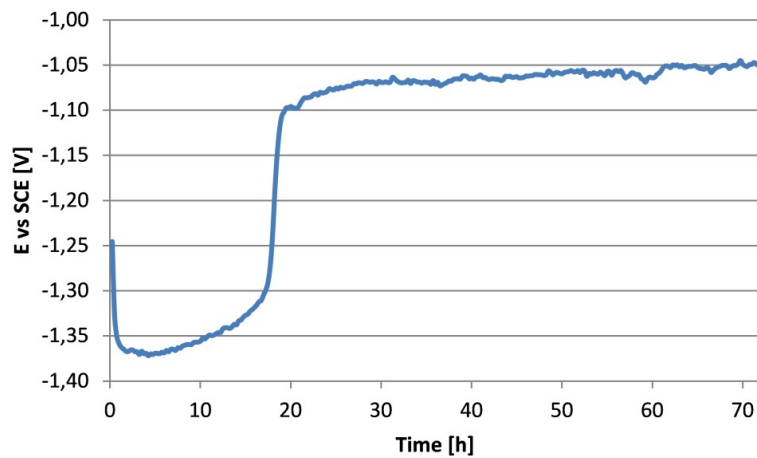

Figure D.1: 100 A/m^2 AC

Figure D.2: 200 A/m^2 AC